Gottfried Wilhelm Leibniz Universität Hannover
Institut für Meteorologie und Klimatologie

Bachelor thesis

LES of a simple block canopy and sensitivity studies with the vegetation model in PALM

by
Hannes Schulz

Supervisor:
Prof. Dr. Siegfried Raasch

Submitted:
May 2012

Abstract

A Large-Eddy Simulation with PALM has been performed of an neutrally stratified, pressure driven turbulent flow above and within a 15 m high idealized homogeneous vegetation canopy. The influence of drag to the flow by the vegetation elements was described by the embedded vegetation model after Watanabe [2004].

Mean profiles and turbulence statistics agree well with results from other LES [Shaw and Schumann, 1992; Su et al., 1998; Watanabe, 2004] and experimental data [Raupach et al., 1996]. The vegetation model could be validated.

Coherent turbulent structures developing according to the mixing-layer analogy [Raupach et al., 1996] were analyzed by calculating turbulence length scales from mean vertical velocity gradients and two-point correlations at the canopy top. The mean spacing between dominant eddies at the canopy top has been found to scale with 2.75 times the canopy height.

Previous studies used a vertical resolution of ten grid points for the canopy layer without giving an explanation why this is necessary. Therefore a sensitivity study was performed to investigate effects of the numerical grid resolution on the model's results, particularly with regard to vertical transports and the spacing between coherent eddies forming from inflection point instabilities at the canopy top.

Analysis of turbulence length scales reveal that resolutions of ten grid points and more lead to similar length scales while lower resolutions lead to different length scales. This indicates that a grid resolution of ten grid points per height of the canopy layer is in fact sufficient, while lower resolutions may cause problematic results.

Contents

List of Figures

List of Tables

List of Abbreviations

S10	Reference simulation with 1.5 m grid spacing
S20	High resolution simulation with 0.75 m grid spacing
S05	Low resolution simulation with 3.0 m grid spacing
ABL	Atmospheric Boundary Layer
CFL	Courant-Friedrichs-Lewy (condition)
HST	Hydrodynamic Stability Theory
IMuK	Institute for Meteorology and Climatology
KH	Kelvin-Helmholtz
LAD	Leaf Area Density
LAI	Leaf Area Index
LES	Large-Eddy Simulation
PALM	PArallelized LES Model
SGS	Subgrid Scale
TKE	Turbulent Kinetic Energy
TS	Tollmien-Schlichting
WT	Wind tunnel

List of Symbols

t	Time
$x, y, z; x_i$	Cartesian coordinates
$u, v, w; u_i$	Streamwise, spanwise and vertical velocity
h	Height of the canopy top
U_h	Mean wind speed at canopy top
$\overline{\psi'\chi'}$	$= \overline{\psi^*\chi^*} + \overline{\psi''\chi''}$ An average turbulent flux of any quantities ψ and χ
g	Gravitational acceleration
f_i	Coriolis parameter
Ω	Rotation period of the earth
ϕ	Geographic latitude
p	Pressure
T	Temperature
θ	Potential temperature
ρ	Density
σ	Standard deviation
r_{ab}	Correlation coefficient of quantities a and b
u_*	Friction velocity
e	Subgrid-scale TKE
k	Wavenumber
ν	Molecular viscosity
a	Leaf area density
λ	Roughness density
c_d	Drag coefficient
c_s	Scalar exchange coefficient
s	Passive scalar concentration
s_c	Passive scalar concentration at a leaf surface
$s_\mathrm{h}, s_\mathrm{top}$	Passive scalar concentration at the canopy top, top of model domain
δ_w	Vorticity thickness
L_s	Shear length scale
Λ_x	Wavelength of/spacing between canopy scale eddies, from mixing layer analogy
Λ_c	Wavelength of/spacing between canopy scale eddies, from integral length scale
$L_w^{\cdot}, L_w^{\cdot\cdot}$	Integral length scale from one- and two-point correlation

1 Introduction

Understanding the biogeophysical cycles on land is crucial for understanding climate and climate change. Forests cover over 42 million km^2 of tropical, temperate and boreal lands, which is over 30 % of the land surface of our planet and they are a breathing lung – influencing the global CO_2 budget [Bonan, 2008].
Forests and other forms of land use with higher vegetation influence exchange processes of momentum, moisture, heat, carbon dioxide, and other chemical species with the atmosphere. The turbulent wind field above a forest drives these exchange processes in the biogeophysical cycles and therefore essentially affects the local weather and climate. The need for more understanding of those exchange processes (e.g. Baldocchi and Meyers [1998]) sparked a wider interest in canopy turbulence 30 years ago [Raupach and Thom, 1981].
Since the early years, a consistent view of the turbulence structures in canopy flows has emerged. Coherent structures are an essential part of it. They are periodically appearing structures that arise from certain mechanisms. The phenomenology of one kind of canopy scale coherent structure is described by the mixing-layer analogy introduced to canopy turbulence by Raupach et al. [1996]. Other, larger coherent structures are in the field of research in recent years, e.g. by Watanabe [2004, 2009] and Su et al. [2000].
Nowadays the attention is directed more and more to the practical realities of canopies on hills, behind windbreaks, near clearings or forest edges, or where the vegetation is sparse and irregular [Finnigan, 2000]. In addition to the interest in the resulting exchange processes, the structure of the turbulent wind field itself needs detailed understanding. An advanced parametrization of orographic roughness has been shown to improve numerical weather prediction models. A hill covered with a vegetation canopy exerts a substantially larger drag on the atmospheric flow than a smoother hill. Another example is the worldwide investment in wind energy turbines sited in regions of mixed topography and forests, so there is a need to develop quantitative understanding of the output of such turbines (see Finnigan and Belcher [2004], and references therein).

Large-Eddy Simulation (LES) has the potential to be the tool of choice modeling the influence of vegetation on the local wind field.

The step into studying complex conditions is best made from a base of firm understanding of canopy turbulence dynamics in simpler situations. Therefore this bachelor thesis will study a turbulent flow above and within a simple horizontally and vertically homogeneous vegetation canopy with the help of a vegetation model coupled to an LES.

2 Motivation and Scope

Today's research in the field of canopy turbulence is motivated by the need for a good understanding of the exchange processes between atmosphere and vegetation, because it is vulnerable for advanced parameterizations of the influence of vegetation in weather prediction and climate models.
LES is the numerical method capable providing data of the turbulent wind field above and within a vegetation canopy at much higher temporal and spacial resolution than possible in field and wind tunnel experiments – and this at reasonable computational costs.

A layer of high vegetation, e.g. a forest or cereal crops, decelerates the flow in the ABL. This becomes visible in a mean wind profile as an inflection point at the top of the vegetation layer. The inflection point induces instabilities to the flow that generate coherent turbulence structures of canopy scale.

While modeling a turbulent flow with the LES technique, scales of turbulence are separated into large and fine structures by a filter. In the LES model used for the simulations in this thesis, PALM (described in Sec. 4), the filter width is equal to the spacing between numerical grid points. The energy containing, larger scales have to be directly resolved by the model equations while the fine structure is parameterized. The parameterization can not handle the larger scales of turbulent motion, its assumptions are only valid for the part of the spectrum where energy is transfered to small eddies and then dissipated to heat. When increasing the grid spacing in order to save computational ressources this has to be checked.

In this Bachelor thesis a sensitivity study is performed to investigate to what extend the resolution of the numerical grid has an influence on the properties of the turbulent flow simulated with PALM. Lower resolutions would permit larger model domains, e.g. for the future study of spatially inhomogeneous canopies, at equally low computation times.
Therefore LES with the vegetation model embedded in PALM are carried out and validated with the results from Watanabe [2004, run III], who gave the outline for the implementation of the vegetation model in PALM. The setup by Watanabe [2004] for an LES of a simple horizontally and vertically homogeneous vegetation canopy in a neutral flow gives also a good possibility to study the features of canopy turbulence in a simple case. The simulations are idealized and resemble a wind tunnel experiment, thus in unlike a neutral atmospheric boundary layer (ABL) the wind direction does not change with height. The results are compared with the experimental data of canopy turbulence statistics from Raupach et al. [1996].

In the next section an overview of today's theoretical understanding of the turbulent flow above and within a canopy is given.

3 Canopy Turbulence

Coherent structures are characteristic for canopy turbulence, the turbulent atmospheric flow in the proximity to a vegetation canopy.
This section will introduce characteristic properties of canopy turbulence and the contemporary understanding of the mechanism developing coherent structures.

3.1 Mixing-layer analogy

Raupach et al. [1996] proposed that near the canopy top the mean velocity profiles as well as the turbulent properties of the flow resemble a plane mixing layer of two coflowing streams with different velocities rather than a near wall boundary layer.
The canopy is a porous drag layer above the solid ground, that decelerates the flow of air. As a result the mean velocity profile has a characteristic inflection point around the canopy top. The inflected wind profile is the key property that distinguishes a mixing-layer flow from a wall boundary layer flow [Raupach et al., 1996].

The canopy layer, roughness and inertial sublayer (see Fig. 1, left) constitute the *inner layer* (often also referred to as surface layer) – approximately the lowest 10 % of the ABL [Garratt, 1980]. The roughness sublayer is reaching up to more than twice the canopy height [Watanabe, 2004]. It can be described as a transition layer between the direct influence of the roughness elements and the inertial sublayer above. In the inertial sublayer profiles approach typical values for the lower ABL [Garratt, 1992]. Discussing the behavior of the turbulent flow properties in section 3.3 will make these sublayers distinguishable.

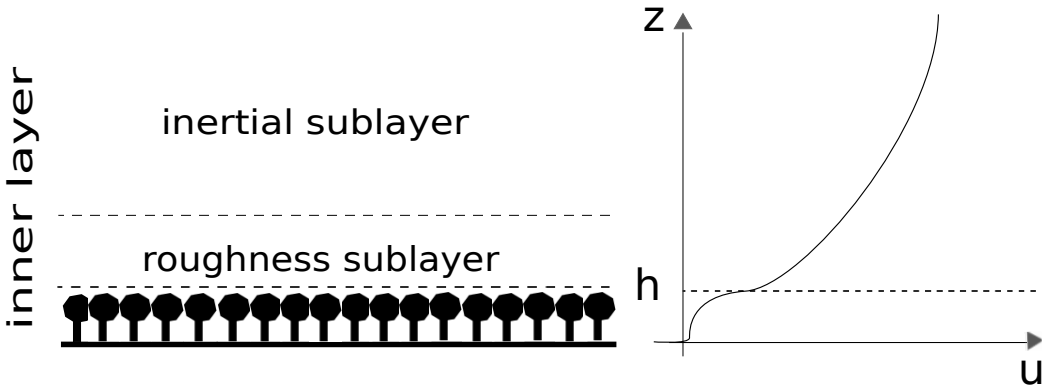

Figure 1: Sketch of the layers in the lower 10% of the ABL above a vegetation canopy of height h. The canopy layer, roughness and inertial sublayer constitute the inner layer (left). A typical inflected wind profile is sketched on the right.

An inflected velocity profile induces characteristic hydrodynamic instability processes which are the cause for the spatial pattern of coherent eddies in a fully developed turbulent flow.

For example, Watanabe [2004, 2009] and Raupach et al. [1996] have shown in their papers that canopy turbulence is in fact quite organized. Coherent eddies of canopy scale dominate the flow in the roughness sublayer and contribute to the bulk of vertical transport in the near surface layer [Raupach et al., 1996]. The formation of coherent structures analogous to a mixing-layer is described in the next part.

3.2 Inflection point instability

An inflection point in the mean streamwise velocity profile at the height of largest shear causes an inviscid instability to small perturbations (e.g. Drazin and Reid [1981]), unlike an uninflected boundary layer profile, which only becomes unstable if viscosity is present. The inflected mean velocity profile is seen as a possible source of the high turbulence intensities in the roughness sublayer.
Using Hydrodynamic Stability Theory (HST), Raupach et al. [1996] show that certain instable modes of perturbations can grow to two-dimensional traverse Kelvin-Helmholtz (KH) waves. The development of these KH waves in a mixing layer between two coflowing streams of velocities u_0 underneath and $u_0 + \Delta u$ above is illustrated in Figure 2.

Figure 2: Instability mechanisms due to an inflected wind profile create Kelvin-Helmholtz waves. A mixing-layer develops between two coflowing air streams of higher velocity above and lower underneath. δ_w describes the thickness of the mixing-layer [Raupach et al., 1996].

A brief description of the universal sequence of instability processes, that leads to the final, fully developed turbulent mixing layer is given in the review paper of Finnigan [2000]. The initial KH waves form traverse vortices that concentrate most of the vorticity induced to the mixing-layer flow by the shear between the two coflowing streams. The mixing layer then undergoes a distinct mixing transition corresponding to the onset of fully developed turbulence and becomes self-preserving (see Finnigan [2000] and references therein). The wavelength of the initial KH waves is maintained throughout the transition process and defines the effective

average streamwise spacing Λ_x of the coherent structures of canopy scale [Finnigan, 2000].

Raupach et al. [1996] introduced the predictor $\Lambda_x/\delta_\mathrm{w}$, known from HST and laboratory experiments of mixing layers, to canopy turbulence. In this ratio, δ_w is the vorticity thickness, a bulk measure for the height of the gradient region between the two coflowing streams. The fact that the unstable eigenmodes in the mixing layer have the same scale as δ_w seems to offer a clue to the origin of the coherent structures. Hence the growing instabilities in the mixing layer are proportional to the magnitude of shear at the inflection point. This can be measured by the shear length L_s scale that Raupach et al. [1996] introduced as:

$$L_\mathrm{s} = \frac{U_h}{\partial u/\partial z|_{z=h}}\,, \tag{3.1}$$

with U_h being the mean velocity at the canopy top. The relation between L_s and δ_w can be derived approximating the vertical gradient of the mean wind component u in equation (3.1) as follows:

$$L_s = \frac{U_h}{\partial u/\partial z|_{z=h}} \approx \frac{U_h}{(U_h-0)/0.5\,\delta_w} = \frac{1}{2}\delta_w\,, \tag{3.2}$$

which holds when shear is maximal at $z = h$ and vanishes with velocities becoming very small within the lower canopy [Raupach et al., 1996]. That velocities vanish to about zero near the ground can be approved form the observation that will be presented in the next part. Raupach et al. [1996] proposed the predictor Λ_x/δ_w for the wavelength of coherent eddies of canopy scale together with equation (3.2) in the form:

$$\Lambda_x = mL_s\,. \tag{3.3}$$

The ratio Λ_x/δ_w is known from experiments and Direct Numerical Simulations to be in the range of 3.5 to 5, resulting in $7 < m < 10$.

3.3 Properties of canopy turbulence

Raupach et al. [1996] accumulated data from wind tunnel and field experiments for their so-called *family portrait* (Fig. 3) of data from turbulence measurements over horizontally extensive, uniform vegetation canopies in a near-neutral flow. It is used in this thesis to explain typical properties of canopy turbulence and to validate the results from the following numerical simulations.

The profiles were obtained form plant canopies like forests and cereal crops, as well as artificial wind tunnel models, spanning a wide range of roughness densities λ, and a 500-fold height range. λ is defined as the total frontal area of canopy elements per unit ground area [Raupach et al., 1996]. Noticeable is that the profiles of horizontal mean velocity, vertical momentum flux, standard deviations of the velocity components and correlation between horizontal and vertical

Table 1: Physical and aerodynamic properties of canopies in different field and wind tunnel experiments; WT = wind tunnel. The roughness density or frontal area index λ is assumed to be half the single-sided leaf area index (LAI) for field canopies [Raupach et al., 1996].

Canopy	Ident	h (m)	λ	U_h/u_*	L_s/h	Reference
WT stripes	A	0.06	0.23	3.3	0.85	Raupach et al. (1986)
WT wheat	B	0.047	0.47	3.6	0.57	Brunet et al. (1994)
WT rods	C	0.19	1	5.0	0.49	Seginer et al. (1976)
Shaw corn	D	2.6	1.5	3.6	0.39	Shaw et al. (1974)
Wilson corn	E	2.25	1.45	3.2	0.46	Wilson et al. (1982)
Moga eucalypt	F	12	0.5	2.9	0.58	Unpublished
Uriarra pine	G	20	2.05	2.5	0.29	Denmead and Bradley (1987)
Amiro aspen	H	10	1.95	2.6	0.58	Amiro (1990a)
Amiro pine	I	15	1	2.2	0.50	Amiro (1990a)
Amiro spruce	J	12	5	2.4	0.44	Amiro (1990a)
Gardiner spruce	K	12	5.1	4.0	0.30	Gardiner (1994)
Baldocchi deciduous	L	24	2.5	2.8	0.12	Baldocchi and Mayers (1988a,b)

velocities have distinctively shaped profiles in common.

For the sake of comparability, the data taken from very different plant canopies have been normalized. The profiles in Figure 3 have been normalized with canopy height h and velocity moments with either $U_h = u(h)$ or the friction velocity $u_* = \sqrt{-\overline{w'u'}}$, which is defined as the square root of minus the turbulent vertical flux of horizontal momentum (e.g. Stull [1988]). u_* was measured in the constant stress layer above the canopy [Raupach et al., 1996]. Details for each experiment are given in Table 1. The profiles are plotted up to $z/h = 2$ which is about the top of the roughness sublayer. All values are time averages, denoted with an overbar.

All mean velocity profiles $u(z)/U_h$ in Figure 3 (a) show a characteristic inflection point right at the canopy top where shear is maximal ($z = h$). Above the canopy the velocity profiles are shaped similar to the logarithmic wind profile in a near wall boundary layer [Kaimal and Finnigan, 1994; Su et al., 1998], whereas wind speed decreases exponentially with depth in the vegetation layer [Raupach et al., 1996].

The drag force constantly maintains the shear between the airflow above and the canopy layer itself where momentum is absorbed by the aerodynamic drag of plant elements, i.e. a vegetation layer is an unlimited sink for momentum. Therefore the profile of normalized momentum flux $-\overline{w'u'}/u_*$ (Fig. 3 b) shows a constant transport of momentum from higher levels (constant stress layer) to the canopy (notice negative sign). The momentum flux decays quite rapidly

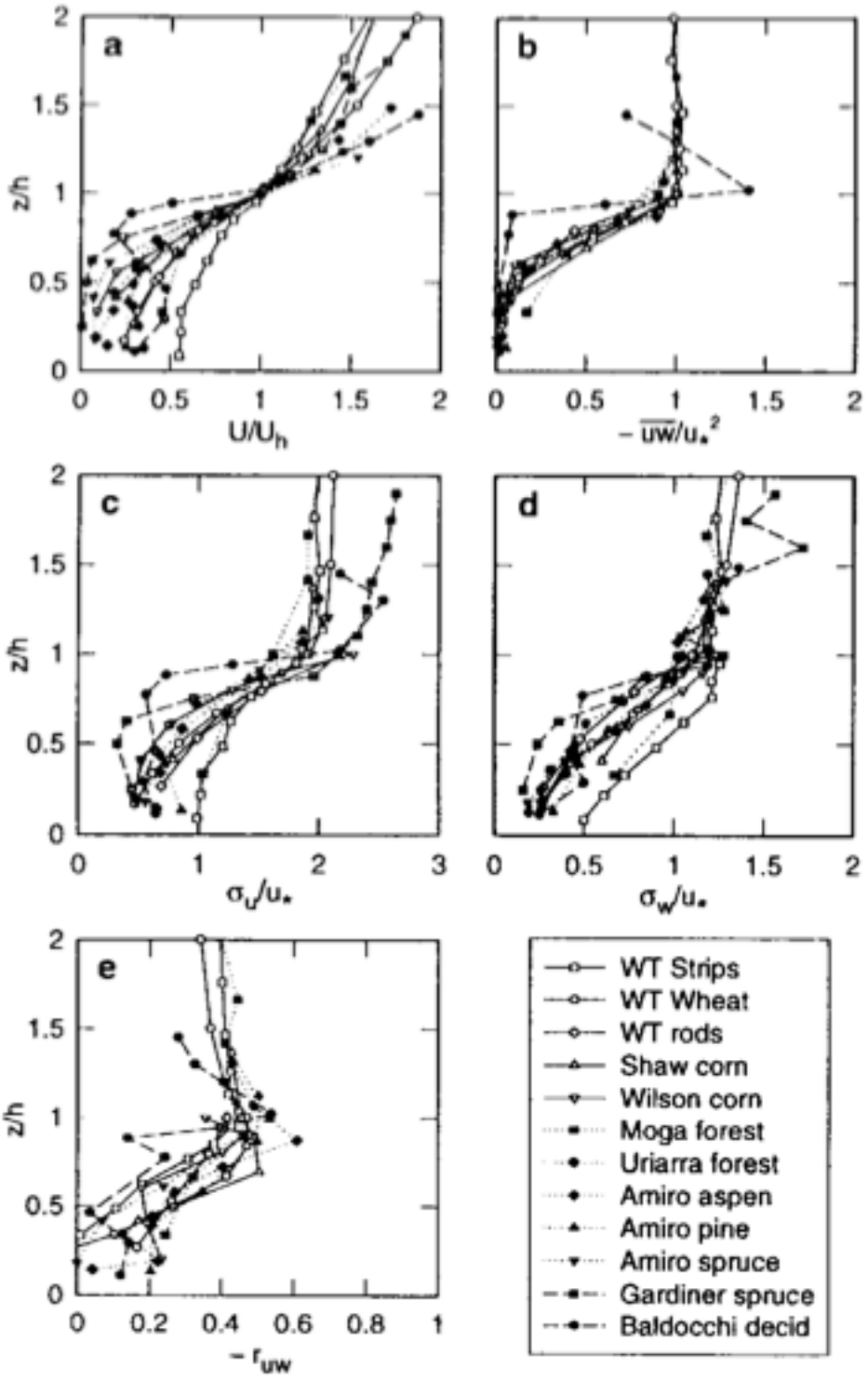

Figure 3: *Family portrait* of canopy turbulence after [Raupach et al., 1996] for canopies A to L listed in Table 1. Profiles with normalized height z/h of: (a) U/U_h; (b) $-\overline{w'u'}/u_*^2$; (c) σ_u/u_*; (d) σ_w/u_* and (e) $-r_{uw} = -\overline{w'u'}/(\sigma_u\sigma_w)$

within the canopy and for all canopy types $-\overline{w'u'}$ decreases to zero by ground level, indicating that all of the vertical and most of the horizontal momentum has been absorbed by the canopy elements [Raupach et al., 1996]. This applies for dense canopies with high roughness density λ (see Tab. 1) as well as for rather sparse canopies.

The profiles of normalized standard deviation of horizontal and vertical velocity σ_u/u_* and σ_w/u_* in Figures 3 (c) and (d) increase above the canopy to values of 2.5 and 1.25, respectively, which are typical values for a constant stress layer [Garratt, 1992]. Within the canopy both profiles vary for different canopy types and the standard deviations decrease to values of about $0.5\,u_*$ in the lower half of the canopy.
The correlation coefficient $-r_{wu} = -\overline{w'u'}/(\sigma_w\sigma_u)$ (Fig. 3 e) reveals a peak in its profile near the canopy top. A value of about 0.5 indicates that turbulence in the proximity of the canopy has a more organized structure [Finnigan, 2000] than it has well above the canopy, where $-r_{wu}$ approaches a value of about only 0.4.

4 Large-Eddy Simulation

All simulations of this thesis were carried out using PALM, a PArallelized LES Model for the study of turbulent processes in the ABL.
PALM is especially designed for the use on massively parallel systems with distributed memory. It has been developed at the Institute of Meteorology and Climatology (IMuK) at the Leibniz Universität Hannover and it is being maintained and improved by the group of Siegfried Raasch[1]. For details on the model and the parallelization see Raasch and Schröter [2001] and references therein.

This chapter provides general information about modeling of turbulent flows using the LES technique. The basic equations with the applied Boussinesq approximation are introduced and the filtering of turbulence scales is explained. An overview of the used methods for numerical discretization in time and space is given and the boundary conditions for this model setup are explained.

4.1 Modeling turbulent flows

It was already indicated in section 3 that the flow in a plant canopy's roughness layer is of turbulent nature. Calculating the Reynolds number, a measure to distinguish between laminar and turbulent flows introduced by Reynolds [1883], proves this observation. The Reynolds number

$$Re = \frac{UL}{\nu_\mathrm{m}} \tag{4.1}$$

is defined as the ratio between inertial and viscous forces. Here U and L are typical the velocity and length scale of the flow and ν_m is the kinematic viscosity. For the latter a typical value for air is about $1.5 \cdot 10^{-5}\ \mathrm{m^2\,s^{-1}}$ [Stull, 1988], hence Re is several orders of magnitude larger than the critical Reynolds number Re_c of about 10^3 for almost all large scale flows in the ABL, with values e.g. of $U = 10\,\mathrm{m\,s^{-1}}$ and $L = 100\,\mathrm{m}$. It is well known from laboratory experiments that when Re_c is exceeded for a flow it can become turbulent.

In order to model a turbulent flow numerically with the LES technique, it is important to understand how much turbulent kinetic energy (TKE) can be associated with a certain range of eddy size. Figure 4 shows schematically the spectral energy density E_sp for a turbulent ABL flow plotted as a function of eddy wavenumber k. The spectrum is divided into three wavelength spans. The production range **P** includes the larger eddies (small wavenumbers). TKE is produced in this range by buoyant forces and shear. Shear extracts energy from the mean flow. For a discussion of the TKE budget equation and its production and dissipation terms see e.g. Kraus [2008, chapter 4] or Stull [1988, chapter 5].

[1] The group's homepage http://palm.muk.uni-hannover.de provides a documentation and further information on PALM

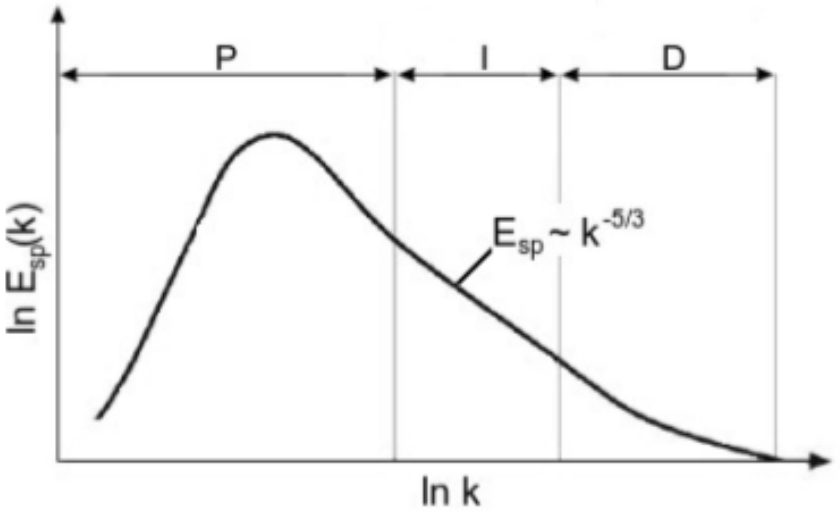

Figure 4: Schematic energy spectrum, divided into **P**roduction range, **I**nertial subrange and **D**issipation range. Indicated is Kolmogorov's minus five-third law in the inertial subrange [Kraus, 2008].

In the inertial subrange **I** larger eddies decay into smaller ones due to instabilities, transferring energy to higher wavenumbers [Kraus, 2008]. There is no production or dissipation within this range. This *energy cascade* satisfies the relation

$$E_{\mathrm{sp}}(k) \sim k^{-5/3}\,, \tag{4.2}$$

known as Kolmogorov's minus five-third law [Kolmogorov, 1941].
In the range of the smallest eddies, TKE is converted into heat by viscous dissipation. For the ABL, Kolmogorov [1941] calculated a scale for the eddies in the dissipation range **D** of about 1 mm, known as the Kolmogorov microscale.

Figure 4 also shows that, represented by the area under the curve, the large, anisotropic eddies contain the bulk of TKE and are responsible for most of the turbulent transport in the boundary layer. Whereas the smaller, isotropic eddies contain a much smaller part of the TKE [Stull, 1988].

PALM is based on the concept of LES and directly simulates scales of turbulence larger than a spatial filter. The unknown influence of turbulence scales smaller than the filter width has to be parameterized. From the discussion above it is clear that the parameterization has to guarantee that the energy is dissipated properly.
If the filter width is too coarse and the energy containing scales of a turbulent flow are not resolved but parameterized, the parameterization will fail to simulate a realistic turbulent flow because it assumes isotropic turbulence.

4.2 Basic equations

The dynamics of a fluid, including turbulence, can be described by a set of prognostic equations in a (x,y,z) Cartesian coordinate frame in a rotating system. The following equations are introduced in tensor notation and with the use of the Levi-Civita symbol ϵ and Kronecker delta δ. The prognostic equations are:

the Navier-Stokes equations for conservation of momentum

$$\frac{\partial u_i}{\partial t} = -u_k \frac{\partial u_i}{\partial x_k} - \frac{1}{\rho}\frac{\partial p}{\partial x_i} - \epsilon_{ijk} f_j u_k - g\delta_{i3} + \nu_m \left(\frac{\partial^2 u_i}{\partial x_k^2} + \frac{1}{3}\frac{\partial}{\partial x_i}\frac{\partial u_k}{\partial x_k} \right) + S_\mathrm{m} \,, \tag{4.3}$$

the continuity equation for conservation of mass

$$\frac{\partial \rho}{\partial t} = -\frac{\partial u_i \rho}{\partial x_i} \,, \tag{4.4}$$

the first principle of thermodynamics

$$\frac{\partial \theta}{\partial t} = -u_k \frac{\partial \theta}{\partial x_k} + \nu_h \frac{\partial^2 \theta}{\partial x_k^2} + S_\mathrm{h} \tag{4.5}$$

and the prognostic equation for the conservation of a passive scalar quantity s

$$\frac{\partial s}{\partial t} = -u_k \frac{\partial s}{\partial x_k} + \nu_s \frac{\partial^2 s}{\partial x_k^2} + S_\mathrm{s} \,. \tag{4.6}$$

The symbol ∂ denotes partial derivatives. u_i are the velocity components u in x- (streamwise), v in y- (lateral) and w in z-direction (vertical). Time is denoted with t. Further, p is pressure, ρ is density of air, θ is potential temperature and g is the gravitational acceleration. The Coriolis parameters $f_i = (0, 2\Omega\cos(\phi), 2\Omega\sin(\phi))$ include the rotation period of the earth Ω and geographic latitude ϕ. The molecular viscosities related to momentum, temperature and scalar quantities are ν_m, ν_h and ν_s, respectively. With the same indices, the S-terms stand for the sum of other sources and sinks.

4.3 Approximation

PALM is using Boussinesq approximated model equations with the local values of thermodynamic variables p, T and ρ being split up into a hydrostatic, stationary base state ψ_0 and a deviation ψ^* of this which is presumed to be much smaller than the base state ($\psi^* \ll \psi_0$). ψ is used synonymously for the variables p, T and ρ. Except for the pressure, the base state is assumed to be horizontally homogeneous.

The advantage of the Boussinesq approximation is the simplification of the continuity equation (4.4), justified for small height intervals where $\rho_0 = \text{const.}$ holds. The divergence of the fluid velocity is zero:

$$\partial u_i / \partial x_i = 0 \,. \tag{4.7}$$

The Navier-Stokes equations (Eq. 4.3) with applied Boussinesq approximation are:

$$\frac{\partial u_i}{\partial t} = -\frac{\partial u_k u_i}{\partial x_k} - \epsilon_{ijk}\, f_j\, u_k - \frac{1}{\rho_0}\,\frac{\partial p^*}{\partial x_i} - \frac{1}{\rho_0}\,\frac{\partial p_0}{\partial x_i} + g\frac{\theta^*}{\theta_0}\delta_{i3} + \nu_m\,\frac{\partial^2 u_i}{\partial x_k^2} + S_\mathrm{m}\,. \tag{4.8}$$

More detailed information on the Boussinesq approximation can be found in Etling [2008, chapter 12] and Stull [1988, chapter 3].

Sound waves have a relatively high propagation velocity. As a consequence of the Boussinesq approximation, the flow becomes incompressible so that sound waves can not exist. In this case, it is possible to choose a larger time step which therefore safes computation time (see Sec. 4.5).

For the separation between resolved scales and the smaller scales according to the LES concept, PALM uses an implicit filtering through the discretization of the model equations on the numerical grid. The volume-balance approach after Schumann [1975] integrates the equations for balance of mass (Eq. 4.7), momentum and the passive scalar as an average over one numerical grid volume.
With ψ used synonymously for any prognostic variable, the quantities in angle brackets $\langle\psi\rangle$ are the resolved volume-averages, while the small scales deviations from this average are marked with double primes ψ''. Because the not directly resolved scales $\psi'' = \psi - \langle\psi\rangle$ are smaller than the grid length they are called Subgrid Scales (SGS). This volume average has the same properties as Reynolds averaging [Schumann, 1975].

Despite the implicit inclusion in energy dissipation, molecular diffusivities ν_ψ are neglected. For the present studies, similar to a wind tunnel experiment, a neutrally stratified and pressure driven flow in the inner layer is simulated. Hence there is no effect of buoyancy. The force driving horizontal momentum is an external pressure gradient F_e with p_e denoting the external pressure field. For the scales of motion in this study, the Coriolis force has little direct impact and therefore it is completely neglected in the Navier-Stokes equations. The filtered forms of the module equations (4.6) and (4.8) are:

the Navier-Stokes-equations

$$\frac{\partial \langle u_i\rangle}{\partial t} = -\frac{\partial \langle u_k\rangle \langle u_i\rangle}{\partial x_k} - \frac{1}{\rho_0}\,\frac{\partial \langle p^*\rangle}{\partial x_i} - \frac{1}{\rho_0}\,\underbrace{\frac{\partial \langle p_\mathrm{e}\rangle}{\partial x_i}}_{F_\mathrm{e}}\,\delta_{i1} - \frac{\partial \langle u_k'' u_i''\rangle}{\partial x_k} - \underbrace{c_d a U \langle u_i\rangle}_{S_\mathrm{m}} \tag{4.9}$$

and the equation for the conservation of a passive scalar

$$\frac{\partial \langle s\rangle}{\partial t} = -\frac{\partial \langle u_k\rangle \langle s\rangle}{\partial x_k} - \frac{\partial \langle u_k'' s''\rangle}{\partial x_k} - \underbrace{c_s a U(\langle s\rangle - s_c)}_{S_\mathrm{s}}\,. \tag{4.10}$$

The unknown SGS fluxes of momentum $\langle u_k'' u_i''\rangle$ and scalar quantity $\langle u_k'' s''\rangle$ have to be parameterized by the SGS-model to reach turbulence closure, i.e. to have no unknown terms that can

not be expressed with the given set of equations. The SGS-model parameterizes the transport of energy from resolved scales to SGS ensuring that energy is dissipated according to the energy cascade. This is realized in PALM according to the model of Deardorff [1980] that determines SGS fluxes with the gradient transport theory using gradients from resolved fields and the eddy diffusivities for momentum:

$$K_\mathrm{m} = c_m l \sqrt{e} \tag{4.11}$$

and for the passive scalar $K_\mathrm{s} = K_\mathrm{m}\,(1 + 2l/\Delta)$, with $e = 1/2\ \langle u_i'' u_i'' \rangle$. $c_\mathrm{m} = 0.1$ is the Smagorinsky constant, l denotes the mixing length and $\Delta = (\Delta x \Delta y \Delta z)^{1/3}$ is the characteristic grid length, which is equivalent to the filter width.
The mixing length l is a measure of the ability of turbulence to cause mixing and it can be interpreted as the distance an air parcel travels before it mixes with the surrounding air [Stull, 1988]. It relates to SGS eddies which are parameterized, therefore l is smaller than the filter width Δ. Also turbulence elements within a distance d from the solid ground can not be larger than d. For neutral stratification the mixing length is calculated in PALM as $l = \min(\Delta, 0.7d)$.
The SGS kinetic energy that is defined above is calculated from the following prognostic equation:

$$\frac{\partial e}{\partial t} = -\frac{\partial \langle u_k \rangle e}{\partial x_k} - \langle u_k'' u_i'' \rangle \frac{\partial \langle u_i \rangle}{\partial x_k} - \frac{\partial}{\partial x_k}\left(\langle u_k'' e \rangle + \frac{\langle u_k'' p'' \rangle}{\rho_0} \right) - \epsilon - \underbrace{2 c_d a U e}_{S_\mathrm{e}} . \tag{4.12}$$

The viscous dissipation ϵ is parameterized as:

$$\epsilon = \left(0.19 + 0.74 \frac{l}{\Delta} \right) \frac{e^{3/2}}{l} . \tag{4.13}$$

Further included are the turbulent fluxes of TKE $\langle u_k'' e \rangle$ and of pressure perturbations $\langle u_k'' p'' \rangle$. To close the model equations, those fluxes are expressed with K_m and the gradient of e in the respective direction.

4.4 Vegetation Model

The additional terms S_m, S_s and S_e in equations (4.9), (4.10) and (4.12) are sink terms which describe the effect of the vegetation elements as in the model of Watanabe [2004].

Vegetation elements like leaves, branches and trunks cause two forms of drag force, form (pressure) drag and skin friction (viscous) drag, that decelerate and alter the airflow. A flow component perpendicular to the surface of a drag element is influenced by a dynamic pressure field in the proximity of the drag element. A component of the flow parallel to the drag element's surface is exposed to viscous drag which provides a direct sink for TKE (e.g. Demtröder [2008]). Form drag transforms large-scale TKE of eddies into small-scale TKE, thereby *short-circuiting* part of the normal eddy cascade and accelerating the dissipation rate for large-scale TKE in the canopy layer [Shaw and Raupach, 1982].

The vegetation elements are described by the model with a leaf area density (LAD) a with unit $\mathrm{m}^2\,\mathrm{m}^{-3}$, multiplied with an isotropic drag coefficient c_d. Together those two quantities are used to parameterize the effect of the vegetation elements per grid volume. No parts of the plants are explicitly resolved.

The drag force S_m by vegetation elements on the instantaneous wind field is proportional to the square of the local velocity, which is represented with the scalar absolute velocity $U = (u^2 + v^2 + w^2)^{1/2}$ and the respective wind component $\langle u_i \rangle$. Drag also acts as sink term S_e for SGS-TKE e [Watanabe, 2004].

The sink or source term for the passive scalar is proportional to an isotropic exchange coefficient of passive scalar for a leaf c_s multiplied with the LAD and the scalar instantaneous local wind speed U. The strength of the sink or source depends on the local gradient $(\langle s \rangle - s_c)$, with the constant level of scalar concentration at a leaf surface s_c [Watanabe, 2004].

4.5 Numerical description and discretization

The prognostic equations must be discretized in space and time in order to solve them numerically. In PALM, the finite differences method that approximates differential operators by a finite difference is used. A Cartesian staggered Arakawa-C grid [Arakawa and Lamb, 1977] is used for the spatial discretization. The grid is illustrated in Figure 5. Scalar quantities are defined at the center of a grid box of volume $V = \Delta x \cdot \Delta y \cdot \Delta z$. Compared to the center position, the velocity components u and v are shifted by minus half a grid length in the respective horizontal direction whereas the w component is shifted by plus half a grid length in vertical direction. Hence, they are defined at the sides of the grid box.

In order to solve the model equations, boundary conditions must be set. The lateral boundaries are periodic, whereas top and bottom boundaries are a frictionless rigid lid and solid ground, respectively. Bottom boundary condition of the horizontal velocity components u and v are no slip (Dirichlet boundary condition). Boundary conditions for horizontal velocities at the top are free slip (Neumann boundary condition). For the passive scalar a constant value was set at both boundaries. For the bottom value of TKE applies a Neumann boundary condition. Values are calculated via the prognostic TKE equation. The necessary initialization profiles and values at the boundaries are discussed in section 5.1.

Between the ground surface and the first prognostic grid level of the horizontal velocity components and scalar quantities ($z = \Delta z/2$) a Prandtl layer is assumed so that vertical turbulent fluxes can be calculated with the similarity theory of Monin and Obukhov [1954] with a prescribed roughness length of $z_0 = 0.005\,\mathrm{m}$.

The advection-scheme used for the present study is the 5^{th} order scheme by Wicker and Skamarock [2002]. Time integration is done by a third-order Runge-Kutta scheme [Baldauf, 2008]. The time step for a numerical model has to fulfill the *Courant-Friedrichs-Lewy* (CFL) condition [Courant et al., 1928] for stable time integration:

$$\Delta t_{\mathrm{CFL}} < \min\left(\frac{\Delta x_i}{\max(\overline{u}_i)}\right) , \tag{4.14}$$

which ensures that information are not transported over more than one grid length during one time step. Further the diffusion criterion [Roache, 1985] ensures that also diffusion of a quantity does not exceed one grid length during the time step:

$$\Delta t_{\mathrm{DIF}} < \min\left(\frac{\Delta x_i^2}{\max(K_{\mathrm{m}}, K_{\mathrm{s}}, K_{\mathrm{h}})}\right) . \tag{4.15}$$

To secure stability of the Runge-Kutta time integration scheme the final time step is reduced by the factor 0.9 and chosen as the minimum of Δt_{CFL} and Δt_{DIF}.

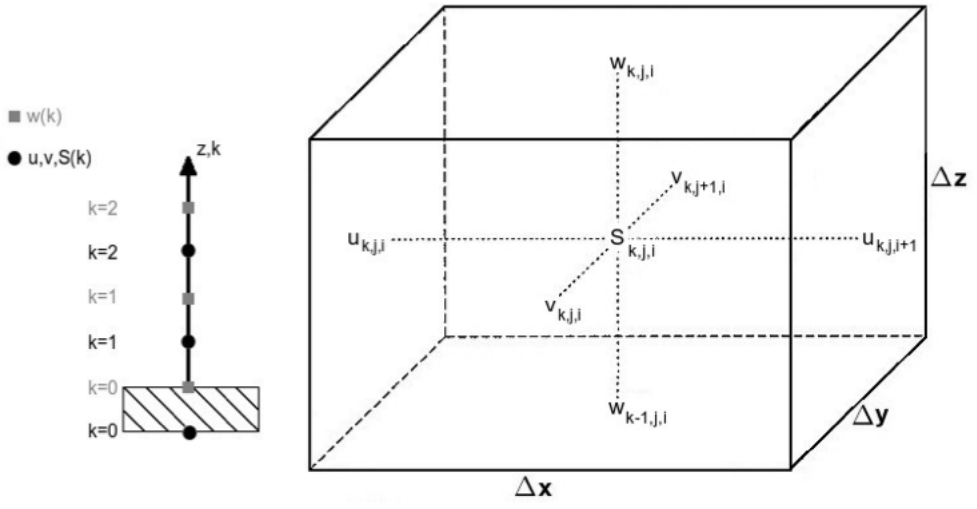

Figure 5: PALM uses an Arakawa-C grid as numerical grid. Scalar quantities are defined at the center of the grid boxes, velocity components at the sides. Compared to the position of the scalar quantity, all velocities u_i are shifted by half a grid length. The lowest level ($k = 0$) where the velocity components are defined is the ground surface (after Sheng et al. [1998]).

5 LES Setup and Validation

This section presents the chosen setup for the LES of a simple block canopy in this thesis. The LES were carried out using PALM and the embedded vegetation model. The current LES were conducted as a re-simulation of the *pressure driven run III* from the paper of Watanabe [2004]. Therefore, the results from Watanabe [2004] are used for a validation of the vegetation model in PALM and the numerical setup chosen for this current study.

5.1 Setup

A *block canopy* is a horizontal extensive layer of drag elements uniformly distributed with height. Other as sketched in Figure 6, there is no explicit trunk space. The drag layer of height $h = 15\,\mathrm{m}$ is described by a constant drag coefficient $c_\mathrm{d} = 0.2$ and a vertical homogeneously distributed LAD a, resulting in a (LAI) of 2 with:

$$LAI = \int_0^h a(z)\mathrm{d}z\,. \tag{5.1}$$

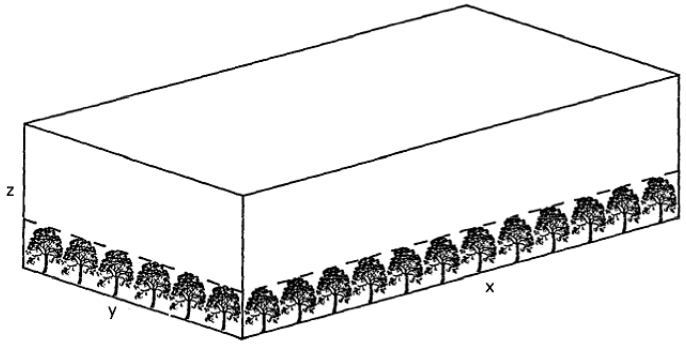

Figure 6: Sketch of the model domain: A forest canopy of height h is simulated in PALM, realized as a uniform block canopy stretching over the whole domain. Drag elements are distributed horizontally and vertically homogeneous [Shaw and Schumann, 1992].

Three simulations under neutral conditions were carried out with different grid resolutions. The model domain was sized 288 m by 288 m by 120 m in streamwise, spanwise and vertical direction, respectively, for all three simulations. This size was chosen according to Watanabe [2004, run III]. Table 2 provides information about the three setups.
An external pressure gradient of $-0.01\,\mathrm{Pa\,m^{-1}}$ in x-direction forced the flow so that the flow at canopy height had an average speed of $u(h) \approx 3.0\,\mathrm{m\,s^{-1}}$. At all times the scalar concentration at the top boundary was held constant at $3\,\mathrm{kg\,m^{-3}}$. The ground surface and all leaf surfaces were held at a concentration value of $1\,\mathrm{kg\,m^{-3}}$ throughout the simulation. Hence, the canopy acted as a sink for the passive scalar that is described in equation (4.10) with the scalar exchange coefficient $c_\mathrm{s} = 0.04$.

Table 2: PALM setup for S10, S20 and S05: S10 is a re-simulation of Watanabe [2004, run III]; S20 and S05 resolve the canopy with twice and half the number of vertical grid points than S10, respectively.

	reference S10	high resolution S20	low resolution S05
$N_x \times N_y \times N_z$	$192 \times 192 \times 80$	$384 \times 383 \times 160$	$96 \times 96 \times 40$
$\Delta x = \Delta y = \Delta z$	1.5 m	0.75 m	3.0 m
grid points			
resolving the forest	10	20	5
grid interval	0.1 h	0.05 h	0.2 h

Figure 7 shows the initialization profiles of the three simulations for streamwise velocity and passive scalar concentration. The values for the different height intervals were adopted from Watanabe [2004], who proposed:

$$\frac{u(z)}{U_h} = \frac{s(z) - s_c}{s_{top} - s_c} = \begin{cases} 1, & z > h\,, \\ 0.2, & z \leq h\,, \end{cases} \qquad (5.2)$$
$$v = w = 0\,.$$

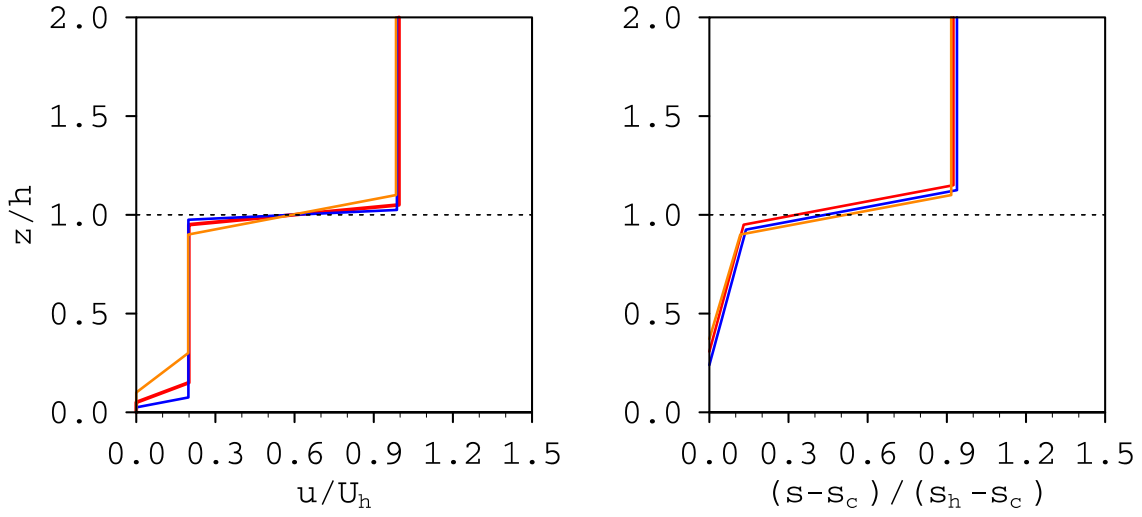

Figure 7: Initialization profiles of streamwise velocity (left) and passive scalar concentration (right) for S10, S20 and S05.

5.2 Validation of the Reference Simulation

From this section on the following notation will be used: for any quantity ψ the resolved part is denoted with an asterisk ψ^* and the SGS part with double quotes ψ''. Time averages are denoted with an overbar $\overline{\psi}$. An average turbulent flux of any quantities ψ and χ is written as $\overline{\psi'\chi'} = \overline{\psi^*\chi^*} + \overline{\psi''\chi''}$. All quantities correspond to a volume average over one grid box, although this is no longer explicitly indicated with angle brackets.

Stationarity and Averaging

The streamwise velocity components for five different heights plotted in Figure 8 suggest that a stationary state is reached after 2 hours of simulated time.
Especially in the upper half of the model domain the time series of the horizontal mean u-component show strong fluctuations around certain niveaus. For lower levels the fluctuations are not as strong and weakest near the canopy, but the timespans at which peaks occur correspond to those observed for higher levels.
There occur intermittent fluctuations with several time spans between 1000 s and 3000 s. These durations have been visually estimated by the author and proved by a spectral analysis (not shown).

Time series of total TKE, i.e. the sum of resolved scale and SGS TKE ($e^* + e$), from horizontal mean values are plotted in Figure 9 for three heights within the canopy layer and above.

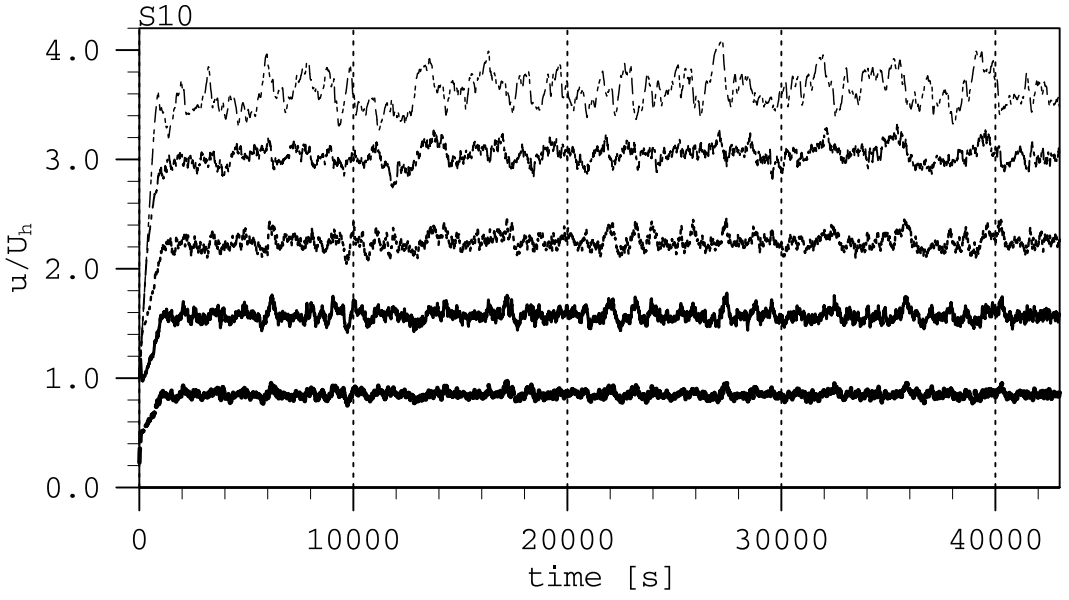

Figure 8: Time series of the streamwise velocity component plotted for heights from 15.75 m (thickest line, lowest niveau), 23.25 m, 38.25 m, 68.25 m to 120.75 m (thinnest line, highest niveau). A stationary period begins after 2 h of simulated time.

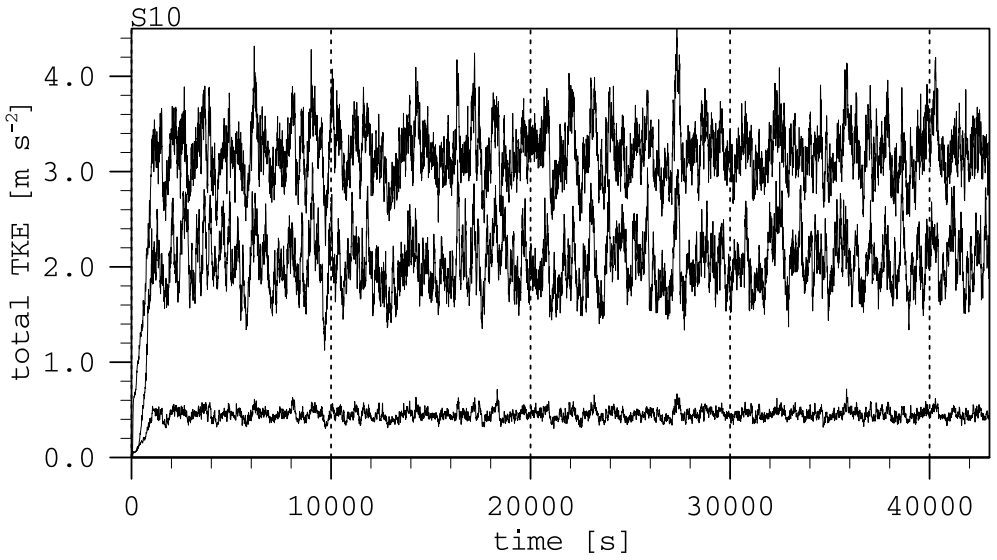

Figure 9: Time series of total TKE plotted for heights 8.25 m (lowest niveau line), 18.75 m (highest niveau line) 71.25 m and (medium niveau line). Note that TKE is maximal in the roughness sublayer and lowest within the canopy layer. A stationary period begins after 2 h of simulated time.

Note that the average niveau of TKE is maximal in the roughness sublayer while it is lower in the inertial sublayer and lowest within the canopy layer. Large fluctuation in the total TKE above the canopy and at higher levels are visible while within the canopy the variance is comparatively small.
Peaks and timespans of these fluctuations correspond to the observations made for the u-component in Figure 8. Apart from turbulence structures with short time scales there exist very large structures that are involved in this long period variations of the streamwise velocity and TKE which make it necessary to use an averaging period of at least 1 hour which should be the minimum that allows to cover one full period of the large variations. In contrast the 2500 s average used by Watanabe [2004] seems rather short assuming that a similar structure of turbulent flow was observed in his LES.

From the TKE approaching a steady mean niveau for each height after less than two hours, choosing a stationary period beginning after two hours of simulated time as suggested above can be affirmed. Also time series of the kinetic energy (turbulent and mean flow kinetic energy; not shown) bear this.

All quantities in the following are averaged over a 6 hour time period beginning after 2 hours of simulated time. A longer averaging interval guarantees better statistics of the intermittent turbulent fluctuations. All profiles are drawn from horizontal mean values and all *mean quantities* are horizontal mean values averaged over 6 hours.

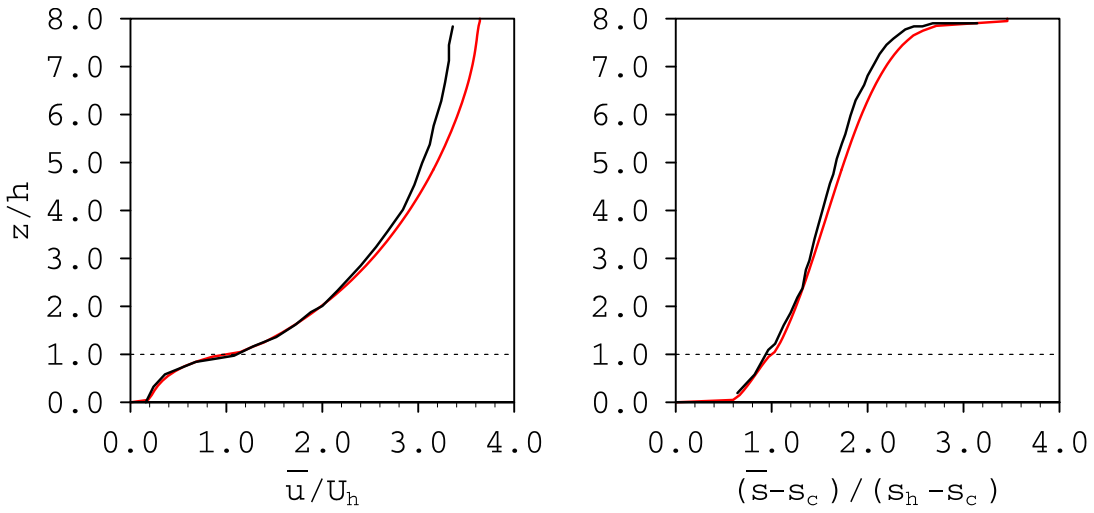

Figure 10: Mean profiles of streamwise wind speed (left) and passive scalar concentrations (right). A red solid line is plotted from data of S10. A black solid line represents results by Watanabe [2004, run III]

Validation of Mean Profiles

The profiles in this part drawn with red lines are based on data from S10. The profiles drawn with black solid lines are from the paper of Watanabe [2004, pressure driven 'run III']. All profiles in this section have been normalized with canopy height h and velocity moments with either the mean wind speed at canopy height U_h or the friction velocity u_*. Values of passive scalar concentrations have been reduced by the surface concentration s_c and normalized by the factor $(s_h - s_c)$ where s_h is the mean concentration at canopy height h.

Vertical profiles of the mean streamwise wind speed are shown in Figure 10 (left). They show the characteristic inflection point at the canopy top where the strongest gradient in the mean velocity profile can be found (height $z = h$ marked with a dashed line). Above the canopy wind speed increases logarithmically, whereas wind speed decreases exponentially with depth in the plant canopy layer. This matches the observations made by Su et al. [1998] and Kaimal and Finnigan [1994].
The normalized profile of mean passive scalar concentrations in Figure 10 (right) shows a gradual increase from the sink within the canopy to the source at the top boundary of the model domain. Near the sink and source the gradients are stronger while in the mid height ranges in between the increase is almost linear.
The passive scalar gets absorbed by plants. In this numerical simulation it fulfills the task of an indicator for vertical transport and mixing due to large eddies. The near linear, weak gradient profile of passive scalar concentration in the middle of the model domain indicates a well mixed

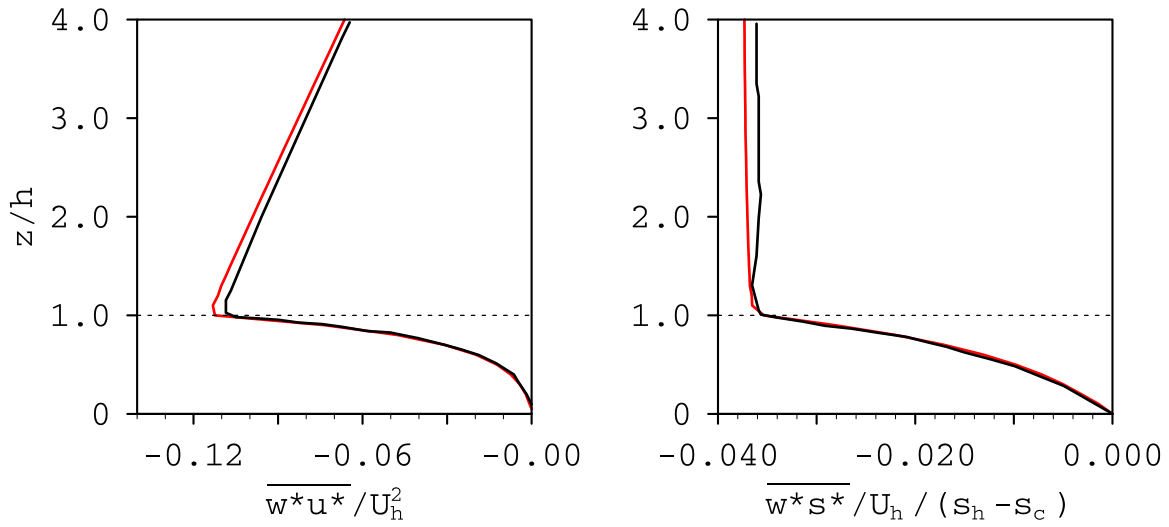

Figure 11: Mean vertical profiles of flux of resolved momentum (left) and passive scalar (right). A red solid line is plotted from data of S10. A black solid line represents results by Watanabe [2004, run III]

layer. The distribution of sources and sinks for the passive scalar in this simulation is similar to that of CO_2 in an ABL including a forest, although a passive scalar may not resemble real trace gases since no chemical processes are described by this model. A passive scalar has no influence on the flow.
Both profiles in Figure 10 are quite similar to the results from Watanabe [2004]. The inflection point is well represented. Also, the wind speeds and passive scalar concentrations within and above the canopy match for heights $z/h < 4$. Above this height the profiles slightly diverge. The different averaging intervals might explain the differences. The shorter averaging interval Watanabe [2004] used is probably not sufficient for the high variability of streamwise wind speed that Figure 8 revealed for higher levels.

Figure 11 shows profiles of vertical turbulent transport of momentum (Reynolds stress) and scalar concentration. Shown are the resolved mean fluxes $\overline{w^*u^*}$ and $\overline{w^*s^*}$. The momentum flux is negative, i.e. the transport is directed downward since the canopy is a sink for momentum due to friction which is proportional to the LAD and drag coefficient.
The average momentum transport is maximal at the canopy top and decreases linearly with height until it vanishes at the top of the model domain ($z/h = 8$ not shown in Fig. 11).
Also the passive scalar is transported with a negative flux from the source at the top boundary to the sink within the canopy layer. The sink for the passive scalar is proportional to the LAD, the exchange coefficient and the local gradient. The average flux observed for the passive scalar is constant above the canopy since there is a constant source at the top boundary and a sink within the canopy layer.

Within the canopy layer, both profiles show the exponential decay expected for the unlimited sink from the discussion in section 3. The linear profiles observed above the canopy indicate that all data were properly sampled during a stationary period and that the averaging interval was chosen long enough.

PALM and the vegetation model can be affirmed as working well from its good agreement with a different numeric model as well as field and wind tunnel experiments especially for the region below $z/h = 4$ that is most interesting for the analysis of coherent structures generated by the wind shear region around the inflection point.
Concluding that S10 is able to reproduce the results from Watanabe [2004, run III], this simulation will be used as the reference simulation for a sensitivity study with different grid lengths.

5.3 2D Cross Sections of velocities and passive scalar concentration

A look at the spacial distribution of velocities and passive scalar concentration might reveal further aspects of the turbulence structure.

Figure 12 displays three instantaneous spatial distributions of streamwise velocity (top), vertical velocity (middle) and passive scalar concentration (bottom) as a vertical-streamwise cross section positioned at 225 m in spanwise direction. Data were taken from S10 at $t \approx 10$ hours.

From the cross sections of the streamwise and vertical wind component in Figure 12 it is obvious that high streamwise velocities are connected with downdraft areas. Pronounced gradients in the streamwise wind component are observed at the interface between updrafts and downdrafts. Therefore regions of great shear also exist well above the canopy and not only where shear is constantly maintained by drag of canopy elements. Strongest shear in the canopy top region is found where large downdrafts touch the canopy.
These large downdrafts highly influence the velocity field near the canopy top but they occur only intermittently. An example for a strong downdraft is visible in Figure 12 at a position of $13 < x/h < 15$, by high streamwise velocities and scalar concentrations. The downdraft impinges the canopy bringing higher velocities and scalar concentrations with it. It is said to *sweep* the canopy layer. Downstream from the sweep region, there is a large updraft region that is tilted in direction of the mean wind. Low velocities and scalar concentrations are found in this *ejection* from the canopy layer.

Figure 13 displays the same instantaneous distributions as Figure 12 but in the horizontal (xy) plane at heights $z = 30.0$ m (w-component) and $z = 30.75$ m (u-component, s). The position of the xz-cross sections is indicated with a dashed line at $y = 225$ m. The correlation between large streamwise velocities as well as high scalar concentrations and downdraft areas is apparent.

The streamwise velocity in Figure 13 reveals elongated zones of high-speed and low-speed motions alternating in spanwise direction. The wavelength of this structure is about the width of the model domain. Figure 21 (appendix) shows that these elongated patterns are still visible in a two hour average of the streamwise velocity. The averaged cross sections of streamwise velocities are calculated at $t = 10$ hours ± 1 hour, so that they correspond to a long term development of the instantaneous pictures shown in this section. Displayed are cross sections for three heights illustrating the vertical extend of these structures.
The elongated regions are most probably caused by Tollmien-Schlichting (TS) waves that develop in a flow with a none constant mean wind profile during the transition process from laminar to turbulent flow [Berlin, 1998; Schlichting and Gersten, 2005]. Such a wind profile is found in any near-wall boundary layer flow, therefore these waves are not connected to the shear region above the canopy. These waves and the elongated structures they cause are rather connected with the start of a numerical simulation or a wind tunnel experiment than a large scale atmospheric flow that is always turbulent (see Sec. 4.1). Therefore the occurrence of these waves is not wanted. From wind tunnel experiments it is known that these turbulent structures will eventually decay after several hours but within the model domain of the current LES they still existed after 12 hours of simulated time. This phenomenon is not fully understood.

Other elongated structures of three dimensional motions, streaks, are known to develop under the influence of strong shear which is found above a canopy, therefore the occurrence of streaks is expected above the canopy [Moeng and Sullivan, 1994; Watanabe, 2009]. The elongated structures visible in Figures 13 and 21 were also found by Watanabe [2004]. The structures were interpreted as streaks, but because the dominant elongated structures observed for all three simulations in this thesis have atypical large dimension and long durability they are probably not connected with streaks. Watanabe [2004] most likely found similar strong elongated circulations developing from TS-waves as found in this thesis.
If the up- and downdrafts connected with streaks are actually important for the formation of large scale coherent structures above a plant canopy, the elongated structures induced by TS-waves are problematic. For the current simulations it is not possible to actually distinguish between the two structures and the features they introduce to the flow.

An animation[2] from vertical-streamwise cross sections at a fixed position in the middle of the model domain was produced for S10. The Animation visualizes the streamwise wind component for one hour of the stationary period. It proves the intermittent occurrence of strong downdrafts. After about 2700 s of simulated time passing in the animation, higher wind speeds emerge within the upper part of the model domain. Strong downdrafts, transporting high velocities to the canopy top, occur much more frequently. This observation is connected with a change in the flow regime at the position of the cross section. The elongated structures are not stable but change in strength and shape. Their relative position stays constant for several hours

[2]The animation is available at: http://vimeo.com/41585586

but as they drift towards the xz-cross section, the area between strong up- and downdrafts, where shear generates large eddies, becomes visible in the cross section.

In contrast to the large scale motions associated with strong downdrafts, the vertical velocity near the canopy top ($z = 30\,\mathrm{m}$) in Figure 13 shows a rather fine-grained structure. Eddies corresponding to this smaller scale are visible in Figure 12 e.g. downstream from about $x/h = 15$. Eddies inducing the dominant vertical perturbations near the canopy top are generated by a KH wave mechanism due to the inflection point in the mean wind profile as discussed in section 3. The mixing-layer analogy does apply to these eddies.

The pronounced shear induced downdrafts, seen in the animation, occur only in between two streamwise elongated up- and downdraft areas, hence horizontal mean values are widely unaffected. Therefore the evaluation of averaged structures near the canopy top should not be affected by the large streamwise elongated structures.

Given that there exist two different mechanisms in the model domain that might generate large scale eddies of which one is not present in natural ABL, large coherent structures cannot be studied from the present simulations. Two averaged lateral-vertical cross sections in Figure 14 show that the average influence of large scale downdrafts near the canopy top, at the height where canopy scale eddies develop due to the shear region above the vegetation layer, is negligibly small. Also the time series of streamwise velocity (Fig. 8, Sec. 5) show that velocity fluctuations are much smaller near the canopy than they are at higher levels.

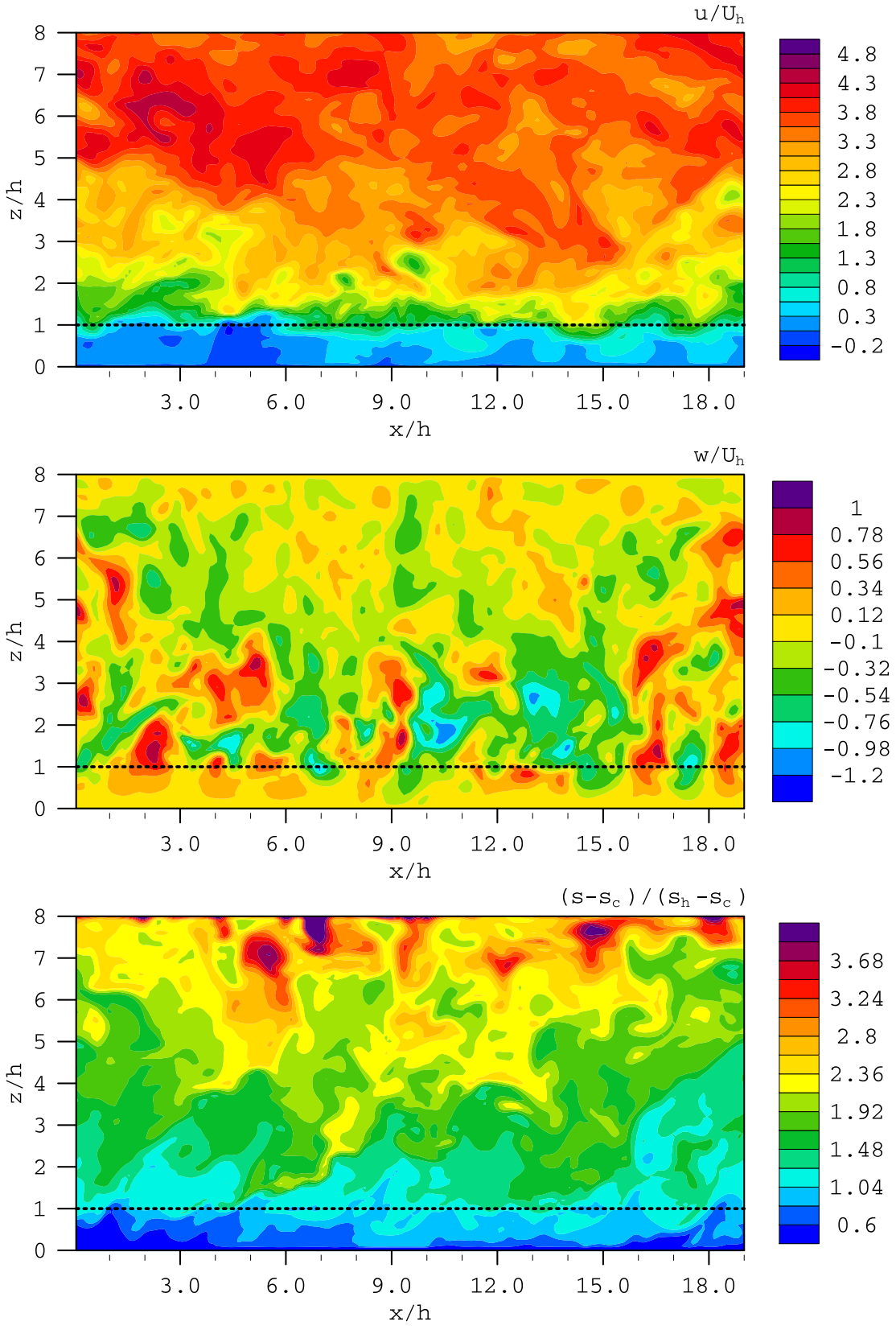

Figure 12: Cross section in the xz-plane at $y = 225\,\mathrm{m}$ showing instantaneous spatial distributions of streamwise velocity (top), vertical velocity (middle) and passive scalar concentration (bottom) from S10. All axes are normalized with h, velocities are normalized with U_h and the passive scalar concentration is reduced by s_c and normalized with $s_h - s_c$. A dashed black line indicates the height of the canopy top.

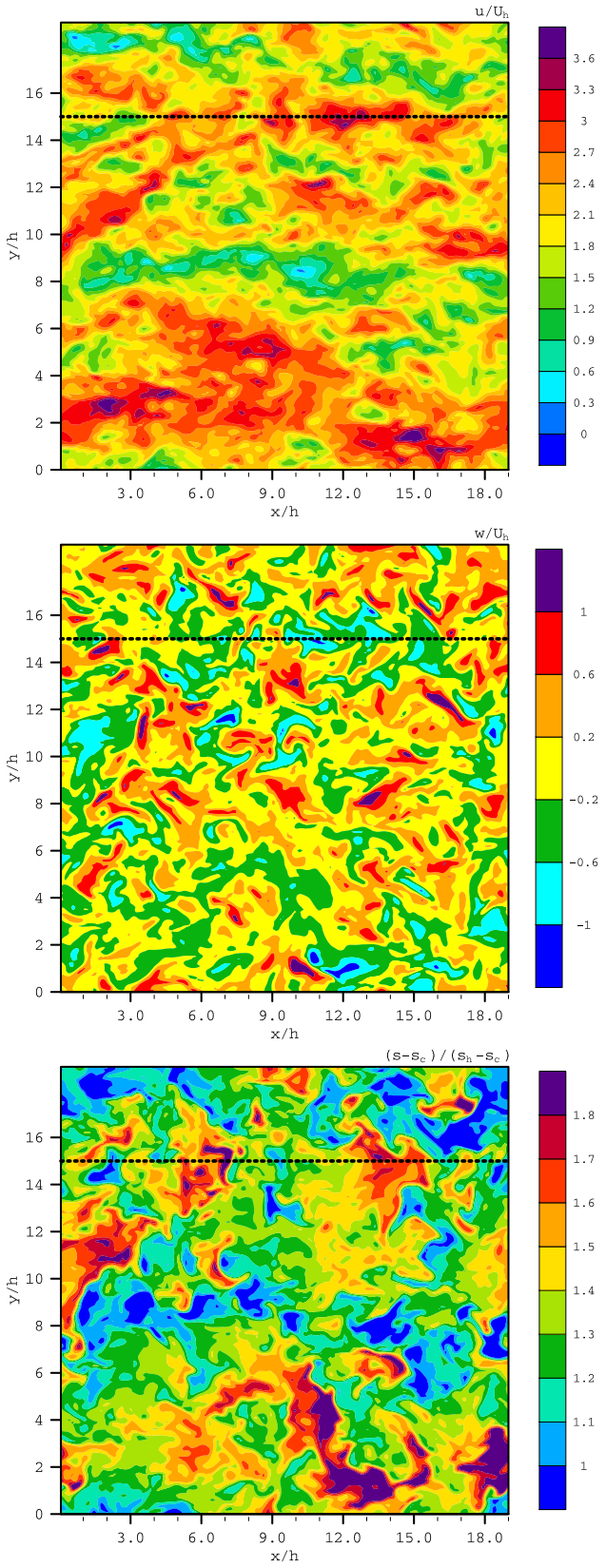

Figure 13: Cross section in the xy-plane at height $z = 30.00\,\mathrm{m}$ (w), $z = 30.75\,\mathrm{m}$ (u, s) showing instantaneous spatial distributions of streamwise velocity (top), vertical velocity (middle) and passive scalar concentration (bottom) from S10. All axes are normalized with h, velocities are normalized with U_h and the passive scalar concentration is reduced by s_c and normalized with $s_h - s_c$. A dashed black line indicates the position of the xz cross section in the model domain.

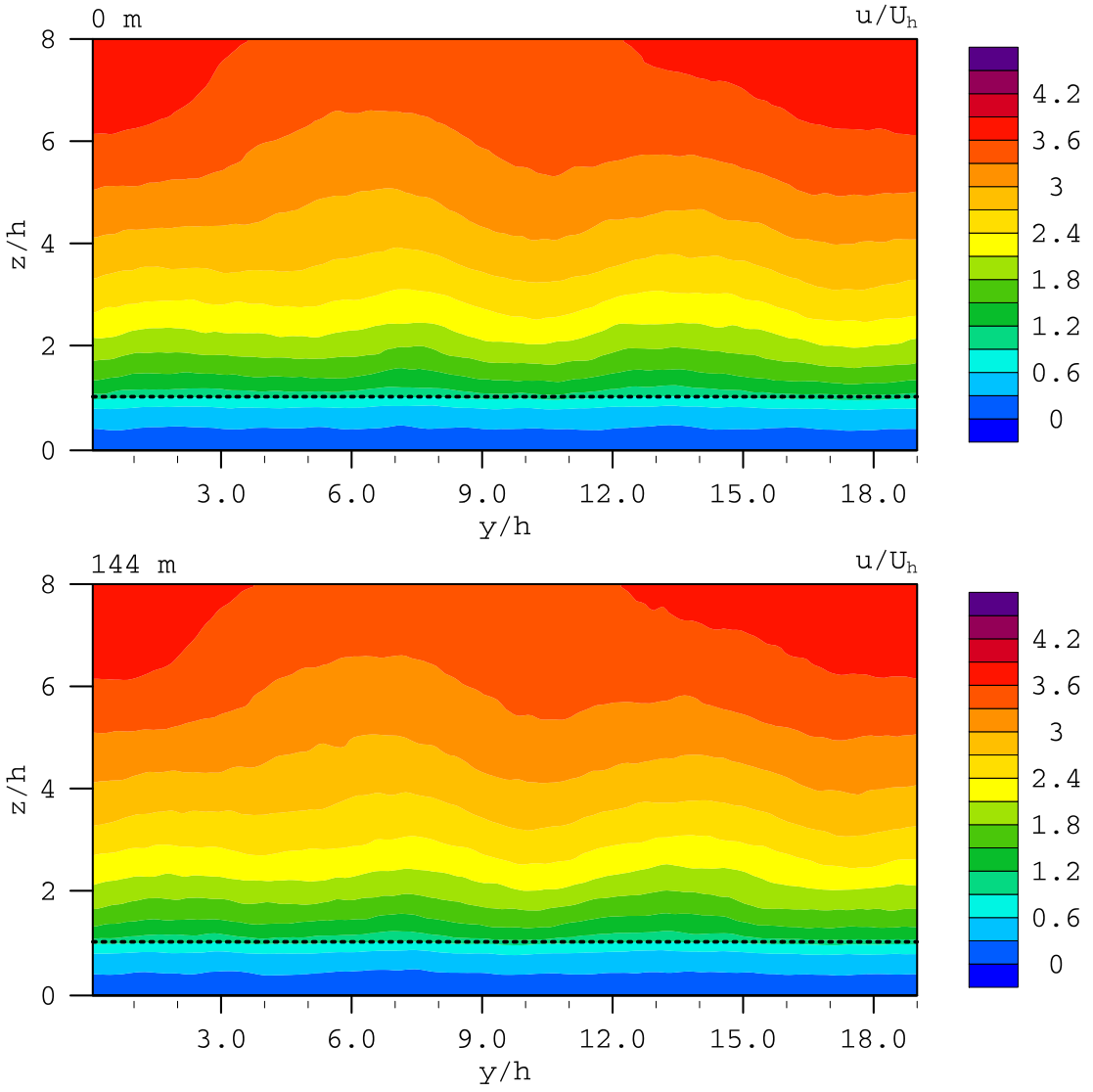

Figure 14: Cross section in the yz-plane at $x = 0\,\mathrm{m}$ and $x = 144\,\mathrm{m}$ showing one hour averages of spatial distributions of streamwise velocity from S10. All axes are normalized with h and the streamwise velocity is normalized with U_h. A dashed black line indicates the height of the canopy top.

6 Results and sensitivity study

The validation with the results from Watanabe [2004] and Raupach et al. [1996] showed that the vegetation model in PALM and the chosen setup is able to reproduce the characteristic mean profiles that are associated with canopy turbulence. The shape of mean profiles of streamwise velocity, turbulent fluxes and turbulence statistics resemble data known from field and wind tunnel experiments.
The three LES setups S10, S20 and S05, different only in the numeric grid length, will be examined in this section to investigate the question to what extend the results of a simple block canopy simulated with the vegetation model in PALM depend on the grid resolution.

6.1 Mean wind profiles

The mean wind profiles obtained from the three simulations are compared with each other. All data from S20 and S05 is also sampled from a stationary period. Stationarity is assured from time series of streamwise wind speeds, kinetic energy and TKE (not shown). All mean values for the three LES correspond to an average of horizontal mean values over 6 hours. Stationarity has also been proved for average profiles. Profiles averaged over several hours (not shown) converge to the profiles shown in this section.
For all three simulations the external pressure gradient driving the flow is set to the same value of $-0.01\,\mathrm{Pa\,m^{-1}}$ (see section 5.1). Also the LAD and drag coefficient is equal for all three simulations so that a mean streamwise velocity at the canopy top of $U_h = 3.0\,\mathrm{m\,s^{-1}}$ was reached for S10, S20 and S05 in the stationary state.

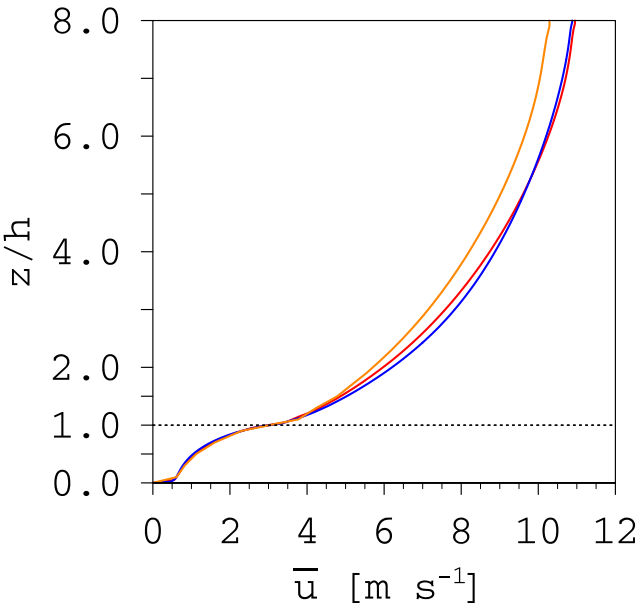

Figure 15: Vertical profiles of mean streamwise velocity for S10, S20 and S05.

The velocity profiles of the three LES in Figure 15 match within the forest. The inflection point is located in between the first grid point above the canopy top and the last within the canopy layer at a height of 15 m. All three LES resemble the shape of the velocity profile in Watanabe [2004, run III].

Above $1.25\,h$ the profile of S05 significantly deviates, it shows lower wind speeds (about $0.4\,U_h$) compared to the other simulations. The profiles from S10 and S20 match quite well but there are slightly higher wind speeds in S20 for heights $2 < z/h < 4$. A possible reason for the significant deviation of S05 will be discussed in the following parts.

6.2 Turbulence statistics

The turbulence statistics calculated from results of this thesis will be compared to those from the experimental data presented in the *family portrait* discussed in section 3.3.

The correlation coefficient between streamwise and vertical velocities (Fig. 16 a) is defined as:

$$r_{wu} = \overline{r}_{wu} = \frac{\overline{w'u'}}{\overline{\sigma}_w \overline{\sigma}_u}\,. \tag{6.1}$$

The observations in the *family portrait* (Fig. 3) show that well above the canopy, r_{wu} approaches values of -0.4. Around the canopy top and in the upper half of the canopy, streamwise and vertical velocity are highly correlated ($r_{wu} < -0.5$). In the current results, the peak in r_{wu} at the canopy top is more pronounced for S05 with a value of -0.7 than for the simulations S10 and S20 with a higher grid resolution, which have a peak value of about -0.65 and -0.6 respectively. The peak of r_{wu} around $z = h$ is connected to the coherent structures forming around the canopy top [Raupach et al., 1996]. The higher (negative) correlation between the u- and w-component reveals a more efficient downward momentum transport. Given a more pronounced peak and an overall higher correlation for S05 above the canopy, the turbulent transport of momentum seems to be more efficient for the simulation with low resolution.

The increase of r_{wu} is almost linear within the lower canopy. The current study as well as other LES of homogeneous block canopies (e.g. Su et al. [1998]) show a higher correlation in the lower half of the canopy layer than derived from observations in the *family portrait*. Most of those measurements where obtained from vegetation layers with an open trunk space, i.e. drag elements in the lower vegetation layer were fewer and different to those at the canopy top, which changes the flow regime so that u- and w-component are less correlated.

The standard deviations for u-,v- and w-component in Figure 16 (b)–(d) are calculated from the respective fluxes, e.g. $\sigma_u = \sqrt{\overline{u'u'}}$. σ_u shows deviations for all three simulations above the canopy. The deviation between S20 and S05 is almost 20 %.
In the lower half of the canopy σ_u and σ_v show higher values for S05 while S10 and S20 are

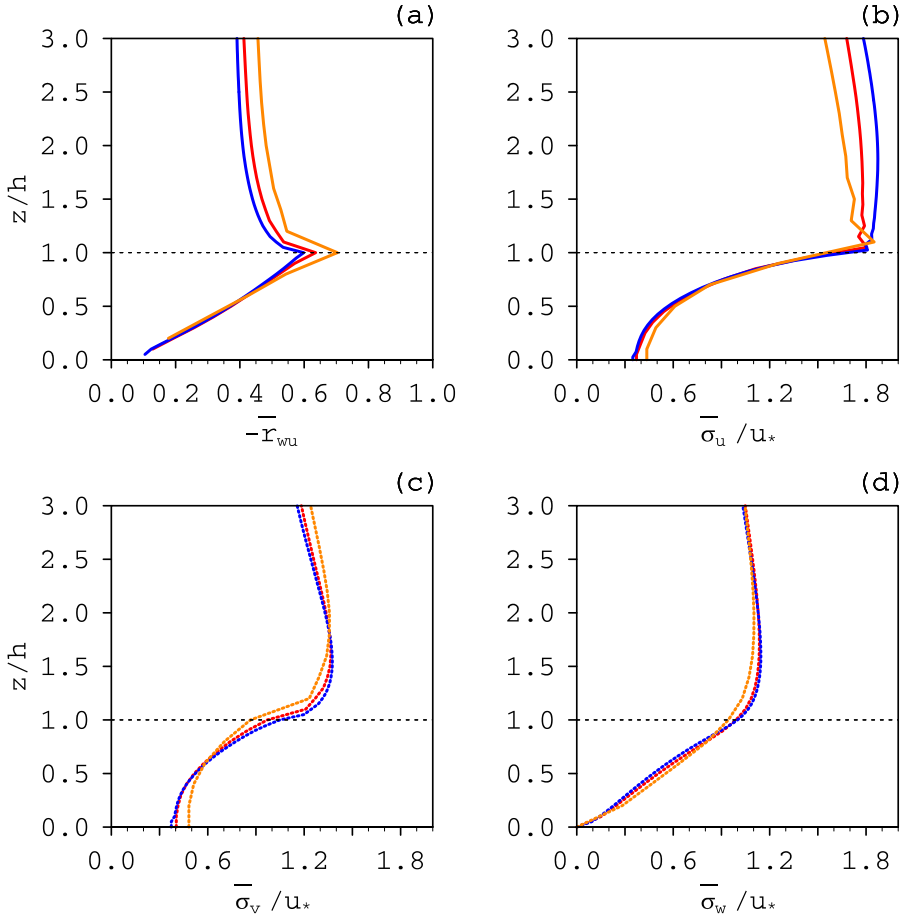

Figure 16: Vertical profiles of the correlation between streamwise and vertical wind component (a), standard deviations for streamwise (b), spanwise (c) and vertical (d) wind component. Values calculated for S10, S20 and S05.

almost equal throughout the canopy layer. σ_w is zero at the ground for all simulations due to the rigid boundary. In the canopy layer and further above there are no significant deviations in this profile. Nevertheless, the profiles for σ_u and σ_w agree well in shape and range of values with the data from field and wind tunnel experiments in the *family portrait*. There is no explicit data for a v-component.

6.3 Comparison of resolved scale and SGS Reynolds stress and TKE

Profiles of the resolved and SGS Reynolds stress are shown in Figure 17 (left). The Reynolds stress (vertical momentum flux) profile has been discussed in section 5.2. The SGS components have a peak at the canopy top, i.e. in the region of greatest shear. They increase proportionally to the grid length, but only make up about 10 % or less of the total flux, which is the sum of resolved and SGS part of the flux.

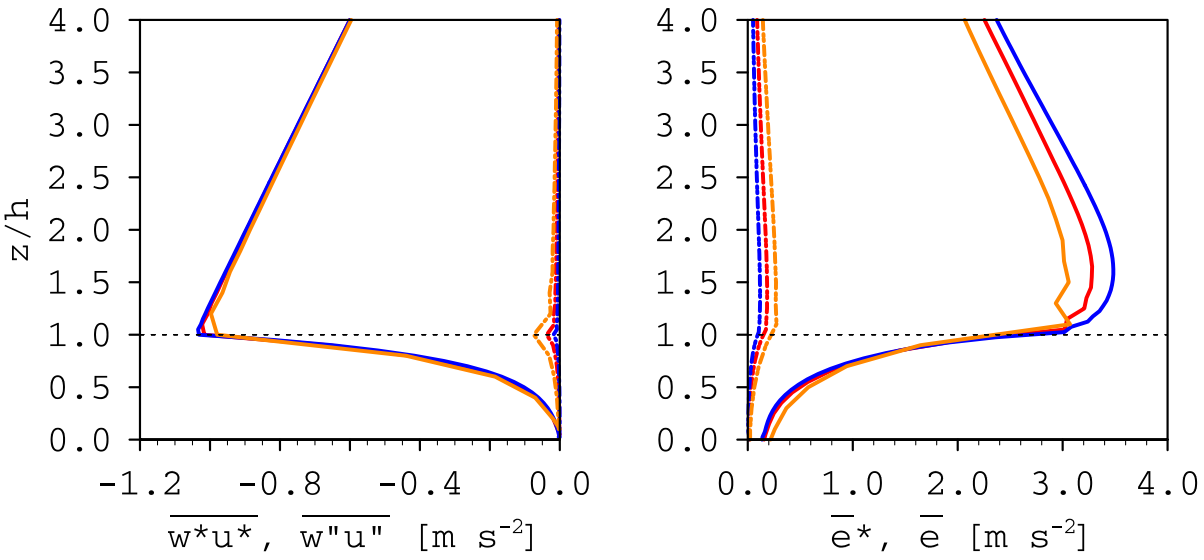

Figure 17: Vertical profiles of resolved (solid lines) and SGS (dashed lines) components of Reynolds stress (left) and TKE (right) for S10, S20 and S05.

The vertical profile of the TKE in Figure 17 (right) of resolved and SGS TKE shows highest values in the roughness sublayer (approximately $1 < z/h < 2$). Within the canopy layer the mean resolved TKE as well as the mean SGS TKE show a rapid decay and both components of TKE are about 10 % of the maximum value at ground level. The SGS TKE is generally less than 10 % of the total TKE.

The SGS components of TKE and Reynolds stress are close to zero near the ground, although generally, the share of the turbulent flow that has to be parameterized near the surface is relatively high because turbulence elements have to get smaller in the proximity to a solid wall. In an LES, the parameterized turbulence is larger than the resolved in a region up to four grid points above the solid ground.
The reason for the decay of the SGS vertical momentum flux near the surface lies within the parameterization of SGS fluxes in the vegetation layer. The SGS fluxes are parameterized using the gradient transport theory (see Sec. 4.3) that approximates the covariances of unknown fluctuations with gradients of known quantities weighted with the corresponding eddy diffusivities. The eddy diffusivities are proportional to the square root of the SGS TKE e (see Sec. 4.2) which is calculated from equation (4.12). For this prognostic equation the vegetation model after Watanabe [2004] adds a sink term for e in a way that drag by canopy elements removes SGS TKE from the flow analogous to the canopy sink term for resolved scale momentum in the Navier-Stokes equations. Hence SGS TKE shows an exponential decay with depth in the canopy layer and the SGS fluxes decay proportionally to the SGS TKE.

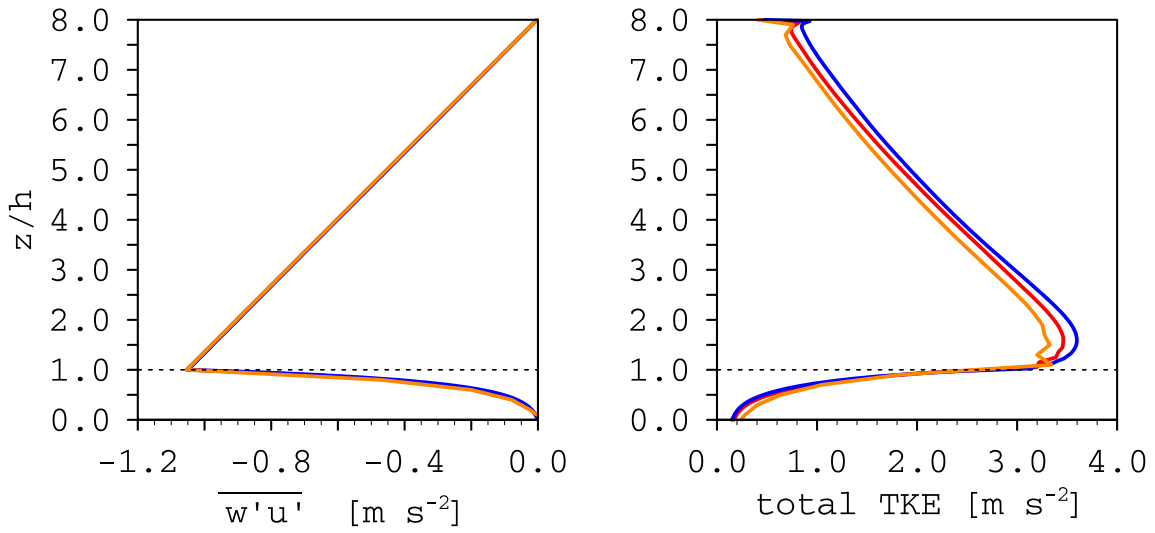

Figure 18: Vertical profiles of total Reynolds stress (left) and TKE (right) for S10, S20 and S05.

In the current simulations a vegetation canopy covers the surface and a volume above it in which all SGS components are forced to decay due to the sink for SGS TKE. This also affects the top of the vegetation canopy where due to the decay of larger turbulence structures to smaller ones (spectral short cut, Sec. 4) an increase of the SGS portion of fluxes would be expected. This might be the area where problems with an insufficient grid resolution occur. The common criteria that the SGS components of turbulent fluxes should be less than 10 % of the total fluxes cannot be used in connection with the vegetation model in order to distinguish between a sufficient and a too coarse model resolution.

Vertical profiles of the total, i.e. resolved plus SGS part, vertical momentum flux and TKE are shown in Figure 18. While the momentum flux is identical for all three simulations, the TKE is significantly lower for S05 in the roughness sublayer. The higher correlation $-r_{wu}$ for S05 (see Sec. 6.2, Fig. 16) suggested a more efficient downward momentum transport from the roughness sublayer into the canopy layer. For S05 the standard deviation of the u-component σ_u, more precisely the fluctuations of u, is lower. Therefore the correlation coefficient $-r_{wu}$ can be higher for this simulation although the momentum flux (covariance) does not show higher values. What could drive a more efficient turbulent transport are larger turbulence structures.

Eddies are contributing to the TKE and its vertical transport from the roughness sublayer into the canopy layer. Together with the faster decay of eddies into small scale turbulence caused by the aerodynamic drag in the canopy, the vegetation model forms a sink for TKE. This sink depends on the numerical grid resolution. As eddies become smaller due to the influence of the vegetation canopy, at one point they become so small that they are seen as deviations from the

volume average over one numerical grid box. From this stage on they have to be parameterized. Since in an LES model with lower grid resolution the point from which on an eddie can no longer be resolved is reached *earlier*, a greater range of the eddy spectrum has to be parameterized. In addition, canopy scale eddies contain a large share of the TKE (see the peak of total TKE situated near the canopy top, Fig. 18). As a consequence, more TKE is taken out of the flow for S05 than for S10 and S20.

Generally the energy dissipation with the parameterization of SGS according to the vegetation model after Watanabe [2004] does work. According to the expectations from the *family portrait*, momentum is absorbed within the canopy layer so that the vertical momentum transport decays to zero within the lower canopy layer. The profiles of total SGS Reynolds stress and TKE in Figure 18 resemble profiles obtained from LES in the papers of Shaw and Schumann [1992] and Su et al. [1998].

6.4 Turbulence length scales

The analysis of vertical profiles of mean streamwise velocity, turbulence statistics, kinetic energy and turbulent fluxes in the previous sections have shown that there is a difference in the vertical transport of momentum for the three LES with different grid resolutions. In this section two turbulence length scales will be used to quantify the size of canopy scale active coherent motions, the dominant eddies responsible for vertical transport near the top of the canopy [Raupach et al., 1996].
The mixing-layer analogy Raupach et al. [1996] introduced to canopy turbulence is a theory on how canopy scale eddies are generated by an inflection point instability mechanism (see section 3). With the shear length scale it is possible to estimate the average spacing between those coherent structures.
Raupach et al. [1996]; Watanabe [2004] and Su et al. [2000] also used integral length scales with single- and two-point autocorrelations of the vertical wind speed to estimate the size of canopy scale eddies.

6.4.1 Shear length scale

The mixing-layer analogy after Raupach et al. [1996] predicts the wavelength or streamwise spacing Λ_x between eddies developed from inflection point instabilities at the canopy top. The vorticity thickness δ_w of the inflected mean wind profile (see Fig. 10) can be expressed with the shear length scale L_s (Eq. (3.2)) which includes the quantities U_h and $\partial\overline{u}/\partial z|_{z=h}$, with values evaluated from profile data of the streamwise velocity $\overline{u}$. Since the actual height h of the canopy top is not matched by the numerical grid, see section 4.5, the gradient of the streamwise wind speed was calculated as a centered difference quotient using the last resolved height in the canopy layer and the first resolved height above (i.e. $h - 0.5\Delta z$ and $h + 0.5\Delta z$).

Table 3: Shear length scale L_s and vorticity thickness δ_w calculated from profile data of the three simulations

	reference	high resolution	low resolution
	S10	S20	S05
L_s	$0.34\,h$	$0.29\,h$	$0.41\,h$
Λ_x	$2.75\,h$	$2.35\,h$	$3.32\,h$
δ_w	10.2 m	8.7 m	12.3 m

The calculated shear length scale for S10 is $L_s = 0.34\,h$. According to the mixing-layer analogy, the streamwise spacing between eddies at the canopy top can be calculated from equation (3.3) as $\Lambda_x = 2.75\,h$, with the factor $m = 8.1$ [Raupach et al., 1996]. The vorticity thickness can be calculated from equation (3.2) as $\delta_w = 10.2\,\mathrm{m}$.
$\Lambda_x = 2.75\,h$ estimated with the mixing-layer analogy is comparable to the streamwise spacing between the two eddy structures found in Figure 12 (middle) around $x/h = 18$. The calculated shear length scale $L_s = 0.34\,h$ is well within the rage of the different values from canopies listed in Table 1. The approximation of the vertical velocity gradient near the inflection point is better the smaller the height intervall between the grid points is. The size of the shear length scale is highly dependent on the discretization of the gradient and therefore it depends on the grid resolution. This restriction applies to numerical models as well as to measurements of L_s in field experiments. It also partly explains the different values of the shear length scale that were obtained from the three simulations with different grid resolution. The values are listed in Table 3.

The wind speed at canopy top U_h is equal for all three LES and the mean wind profiles for heights $z/h < 1.25$ in Figure 15 match. Therefore in a sense the prediction of an increasing spacing between canopy scale eddies with decreasing grid resolution seems confusing. But not only this calculation method for L_s is based on an approximation of the gradient at the canopy top but also PALM solves the equations with information from a discrete numerical grid. Whether the weaker resolved vertical velocity gradient has a physical meaning and causes larger canopy scale eddies, as predicted by the shear length scale, will be verified in the next section by a different method to quantify the streamwise spacing of coherent structures.

6.4.2 Integral length scales

Integral length scales, defined as the integral over the mean autocorrelation function, can be used to describe the spacing between coherent structures. In this section they will be used to analyse the streamwise spacing between canopy scale eddies.

The autocorrelation function that will be used is a function of spatial lag. The first zero

crossing of the mean autocorrelation function describes the average distance after which the airflow's movement is no longer influenced by the same eddy structure.

There are two concepts of autocorrelation functions. One correlates values from a single point in space lagged in time and the other correlates values from two points in space, separated by a spatial lag, at a fixed time. Two-point correlations can give direct information on the size of turbulence structures. Single-point correlations have to assume, according to Taylor's hypothesis of frozen turbulence [Taylor, 1938], that a turbulence structure does not change while it is advected with the mean wind past a sensor. To calculate the size of this structure, the timespan (i.e. maximal time lag) while the structure's signal can be seen in the autocorrelation function is taken and multiplied with the mean wind speed.

The term *canopy scale eddies* arises from single-point measurements. Raupach et al. [1996] calculated the single-point integral length scale

$$L_w^{\cdot} = \overline{u}(z)\frac{1}{\sigma_w^2(z)}\int_0^\infty \overline{w'(s)w'(s+t)}\,\mathrm{d}t \tag{6.2}$$

from time-lagged data and showed that $L_w^{\cdot}$ is about $0.33\,h$ and the corresponding length scale of the streamwise component $L_u^{\cdot}$ is about $1\,h$ at height $z = h$. This indicates, as quoted in section 3, that eddies responsible for the bulk of vertical transport (active turbulence) at the canopy top, scale with height h [Raupach et al., 1996]. Eddies which are much larger than h in their vertical extend are practically horizontal near the canopy top, because of the constraints of continuity and the ground surface. Therefore, eddies with vertical length scales L_w much greater than h can contribute little to the vertical transport [Raupach et al., 1996].

Although most experimental data is based on single-point measurements, and calculated as in equation (6.2), whenever possible information on turbulence length scales should not be obtained from single-point correlations. With generally high turbulence intensities involved in canopy turbulence, Taylor's hypothesis of frozen turbulence is violated [Breitenbach, 2009; Shaw et al., 1995]. Therefore the two-point integral length scale will be used in addition to the shear length scale to measure the streamwise wavelength of canopy scale eddies, defined by [Watanabe, 2004] as:

$$\Lambda_c(z) = 2\pi L_w^{\cdot\cdot}(z) = 2\pi\int_0^\infty r_{ww}(r_x, z)\,\mathrm{d}r_x\,, \tag{6.3}$$

with r_{ww}, the horizontal two-point autocorrelation function for vertical velocities:

$$r_{ww}(r_x, z) = \frac{\overline{w'(x+r_x, y, z, t)w'(x, y, z, t)}}{\sigma_w^2(z)}\,. \tag{6.4}$$

r_x is the horizontal spatial lag in streamwise direction. r_{ww} is horizontally averaged. The first zero crossing of the correlation function is chosen as the upper boundary for the integral. The correlation function for S20, S10 and S05 is plotted in Figure 19. The result for S10 is

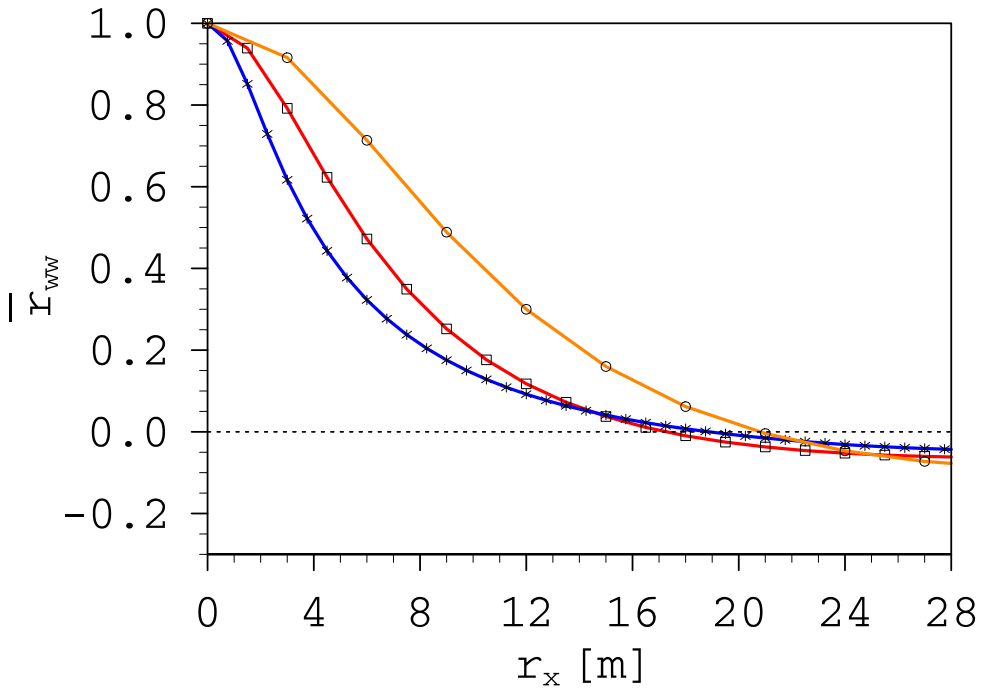

Figure 19: Two-point correlation function for S10, S20 and S05.

$\Lambda_c = 2.74\,h$, which is in excellent agreement with $\Lambda_x = 2.75\,h$ from the mixing-layer analogy.

The turbulence length scale has also been calculated for S20 and S05. The mean streamwise spacings Λ_c from two-point correlation are listed in Table 4. Figure 20, taken from the paper of Raupach et al. [1996], is a scatter plot of streamwise spacing, mostly obtained from single-point correlations, against shear length scale, both normalized with h. L_s and Λ_c from the three current simulations of this thesis are mapped in this scatter plot. They all lie within the scatter, S10 and S20 even close to each other on the regression line. S05 is not as close to the regression line and the position of the other two simulations in the scatter plot.
The fact that the results for L_s and Λ_c match experimental data gives prove to the thesis that the calculated turbulence length scales are not influenced by the large streamwise elongated structures that are connected to the transition from laminar to turbulent flow which does not occur within the ABL.

Table 4: Two-point integral length scales calculated for S10, S20 and S05

	reference	high resolution	low resolution
	S10	S20	S05
Λ_c	$2.74\,h$	$2.22\,h$	$3.95\,h$

The two-point correlation for S05 is calculated with rather few data points compared to the other two simulations. A higher grid resolution guarantees more statistical significance for the integral length scales. When choosing the grid resolution for an LES this should also be considered.

Λ_c calculated from the shear length scale and Λ_x from two-point integral time scales suggest that the actual canopy scale eddies are larger for S05. Larger turbulence structures and thus a more *organized* flow might in fact drive the more efficient vertical transport of momentum.

6.5 Conclusions from sensitivity study

Sections 5.2 and 6 showed that the vegetation model in PALM together with the chosen model setup is able to reproduce the results from Watanabe [2004, run III]. The results from this paper can be integrated into the contemporary physical picture of canopy turbulence that is known from field and wind tunnel experiments (Raupach et al. [1996] and references therein) and LES studies (Shaw and Schumann [1992]; Watanabe [2004, 2009] and Su et al. [2000, 1998]).

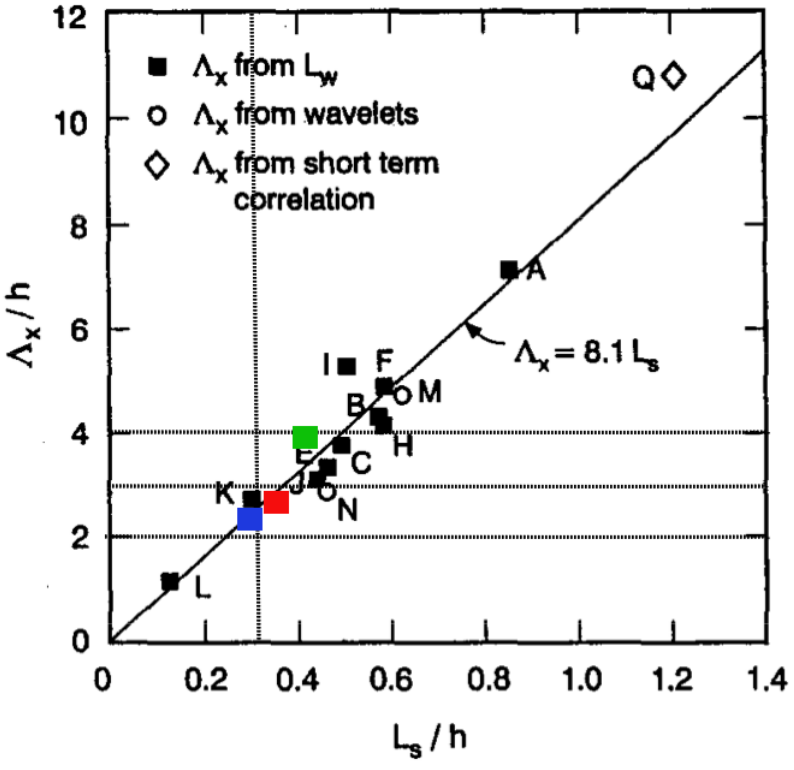

Figure 20: A scatter plot of streamwise spacing Λ_x against shear length scale L_s, both normalized with h obtained from experimental data (after Raupach et al. [1996]). The factor $m = 8.1$ used in the Mixing-layer analogy is taken from the linear regression. For a description of the data of points A–L see Table 1. L_s and Λ_c from S10, S20 and S05 are mapped in the scatter plot.

From mixing-layer theory and two-point integral length scales (Sec. 6.4) the spacing between canopy scale eddies was found to be 2.75 times the height of the canopy.

S10 and S20 showed very similar results. From the overall picture of the results in this section, the scale of active canopy turbulence actually seems to be larger for S05. Especially the two-point integral length scales have given proof that the average spanwise spacing between canopy scale eddies is larger in S05 than it is in the other two simulations. Overall lower wind speeds above the canopy seem to be caused by a more efficient vertical transport with larger eddies. The shear length scale, as a very simple measure for the size of eddies generated by inflection point instability, already gave a hint to that.

7 Summary

The sensitivity study on the influence of the resolution of the numerical grid showed that a finer grid length than $0.1\,h$ is not necessary for canopy turbulence studies, although this might only be valid for the simple case of a homogeneous block canopy. A lower resolution than a grid length of $0.2\,h$ should probably not be chosen.
The study also uncovered a much more complex picture than expected. The common criteria that SGS components should be less than $10\,\%$ of the total fluxes and TKE to distinguish between a sufficient and a too coarse grid resolution can not be used in connection with the vegetation model. In addition to be able to resolve the energy containing scales of turbulence, it also seems important to resolve the canopy layer with sufficient grid points to model the generation and also decay of eddies in a right way.

To finally reject the possibility to choose a grid resolution that has as little as five grid points to resolve turbulence within the canopy layer, it has to be assured that the large streamwise elongated structures observed in the model domains of all three simulations do not influence canopy turbulence. Therefore further LES are necessary in which it is tried to get rid of these structures
Unfortunately, further simulations could not be made during the time given for this Bachelor thesis.

Acknowledgements

First of all, I would like to thank Siegfried Raasch, Farah Kanani and the whole PALM workgroup for your time, good advice, guidance and supervision. Thank you for the help finding my errors and for the hints to solve technical problems. Without the motivating discussions which supported the progress of this bachelor thesis it would all not have been possible. Thank you lots!

Also I have to thank my family and friends for keeping me sane. Thank you for not minding my bad mood and the little time I had for every one of you. Thanks for your encouragement and help. And last but not least, I am very grateful to everyone who corrected my thesis and gave hints for improvement. This was great help. Thanks for your time. I owe you a beer or two!

Eidesstattliche Erklärung

Hiermit erkläre ich, dass ich die vorliegende Bachelorarbeit selbstständig und nur unter Verwendung der angegebenen Quellen und Hilfsmittel sowie dem Rat meiner akademischen Lehrer angefertigt habe.

Hannes Schulz

References

Arakawa, A. and Lamb, V. R. (1977). Computational design of the basic dynamical processes of the UCLA general circulation model. *Methods of Computational Physics*, 16:173–263.

Baldauf, M. (2008). Stability analysis for linear discretisations of the advection equation with Runge-Kutta time integration. *Journal of Computational Physics*, 227:6638–6659.

Baldocchi, D. and Meyers, T. (1998). On using eco-physiological, micrometeorological and biogeochemical theory to evaluate car- bon dioxide, water vapor and gaseous dep- osition fluxes over vegetation. *Agricultural and Forest Meteorology*, 90:1–25.

Berlin, S. (1998). *Oblique Waves in Boundary Layer Transition.* PhD thesis, Kungl Tekniska Högskolan, Stockholm.

Bonan, G. B. (2008). Forests and climate change: Forcings, feedbacks, and the climate benefits of forests. *Science*, 320:1444–1449.

Breitenbach, Y. (2009). Die Prüfung der Taylor-Hypothese in der städtischen Grenzschicht mittels Grobstruktursimulation. Master's thesis, *Institut für Meteorologie und Klimatologie, Universität Hannover.*

Courant, R., Friedrich, K., and Lewy, H. (1928). Über die partiellen Differenzengleichungen der mathematischen Physik. *Mathematische Annalen*, 100:32–74.

Deardorff, J. W. (1980). Stratocumulus-capped mixed layers derived from a three-dimensional model. *Boundary-Layer Meteorology*, 18:495–527.

Demtröder, W. (2008). Experimentalphysik 1. *Springer, Berlin*, 5th Ed., 513 pp.

Drazin, P. G. and Reid, W. H. (1981). Hydrodynamic Stability. *Cambridge University Press, New York*, 2nd Ed., 605 pp.

Etling, D. (2008). Theoretische Meteorologie. *Springer, Berlin*, 3rd Ed., 376 pp.

Finnigan, J. J. (2000). Turbulence in plant canopies. *Annual Review of Fluid Mechanics*, 32:519–571.

Finnigan, J. J. and Belcher, S. E. (2004). Flow over a hill covered with a plant canopy. *Quarterly Journal of the Royal Meteorologycal Society*, 130:1–29.

Garratt, J. R. (1980). Surface influence upon vertical profiles in the atmospheric near-surface layer. *Quarterly Journal of the Royal Meteorological Society*, 106:803–819.

Garratt, J. R. (1992). The atmospheric boundary layer. *Cambridge University Press, New York*, 1st Ed., 316 pp.

Kaimal, J. C. and Finnigan, J. J. (1994). Atmospheric boundary layer flows: Their structure and measurement. *Oxford University Press, New York*, 1st Ed., 289 pp.

Kolmogorov, A. N. (1941). The local structure of turbulence in incrompressible viscous fluid for very large Reynolds numbers. *Doklady Akademii Nauk SSSR*, 32:299–303.

Kraus, H. (2008). Grundlagen der Grenzschicht-Meteorologie. *Springer, Berlin*, 1st Ed., 214 pp.

Moeng, C.-H. and Sullivan, P. P. (1994). A comparison of shear- and buoyancy-driven plantetary boundary layer flows. *Journal of Atmospheric Science*, 51:999–1022.

Monin, A. S. and Obukhov, A. M. (1954). Basic laws of turbulent mixing in the surface layer of the atmosphere. *Doklady Akademii Nauk SSSR*, 24:163–187.

Raasch, S. and Schröter, M. (2001). PALM – A large-eddy simulation model performing on massively parallel computers. *Meteorologische Zeitschrift*, 10(5):363–372.

Raupach, M. R., Finnigan, J. J., and Brunet, Y. (1996). Coherent eddies and turbulence in vegetation canopies: the mixing-layer analogy. *Boundary-Layer Meteorology*, 78:351–382.

Raupach, M. R. and Thom, A. S. (1981). Turbulence in and above plant canopies. *Annual Review of Fluid Mechanics*, 13:97–129.

Reynolds, O. (1883). An experimental investigation of the circumstances which determine whether the motion of water shall be direct or sinuous, and of the law of resistance in parallel channels. *Philosophical Transactions of the Royal Society of London*, 174:935–982.

Roache, P. J. (1985). Computational fluid dynamics. *Hermosa Publishers, New York*, 6th ed., 446 pp.

Schlichting, H. and Gersten, K. (2005). Grenzschicht-Theorie. *Springer, Berlin*, 10th Ed., 799 pp.

Schumann, U. (1975). Subgrid scale model for finite difference simulations of turbulent flows in plane channels and annuli. *Journal of Computational Physics*, 18:376–404.

Shaw, R. and Schumann, U. (1992). Large-Eddy Simulation of turbulent flow above and within a forest. *Boundary-Layer Meteorology*, 61:47–64.

Shaw, R. H., Brunet, Y., Finnigan, J. J., and Raupach, M. R. (1995). A wind tunnel study of air flow in waving wheat: two-point velocity statistics. *Boundary-Layer Meteorology*, 76:349–376.

Shaw, R. H. and Raupach, M. R. (1982). Averaging procedures for flow within vegetation canopies. *Boundary-Layer Meteorology*, 22:79–90.

Sheng, J., Wright, D. G., Greatbatch, R. J., and Dietrich, D. E. (1998). CANDIE: A new version of the DieCAST ocean circulation model. *Journal of Atmospheric and Oceanic Technology*, 15:1414–1432.

Stull, R. B. (1988). An introduction to boundary layer meteorology. *Springer, New York*, 13th Ed., 670 pp.

Su, H.-B., Shaw, R. H., and U, K. T. P. (2000). Two-point correlation analysis of neutrally stratified flow within and above a forest from Large-Eddy Simulation. *Boundary-Layer Meteorology*, 49:423–460.

Su, H.-B., Shaw, R. H., U, K. T. P., Moeng, C.-H., and Sullivan, P. P. (1998). Turbulent statistics of neutrally stratified flow within and above a sparse forest from Large-Eddy Simulation and field observations. *Boundary-Layer Meteorology*, 88:363–397.

Taylor, G. (1938). The spectrum of turbulence. *Proceedings of the Royal Society*, A164:476–490.

Watanabe, T. (2004). Large-Eddy Simulation of coherent turbulence structures associated with scalar ramps over plant canopies. *Boundary-Layer Meteorology*, 112:307–341.

Watanabe, T. (2009). LES study on the structure of coherent eddies inducing predominant pertubations in velocities in the roughness sublayer over plant canopies. *Journal of the Meteorological Socienty of Japan*, 87(1):39–56.

Wicker, L. J. and Skamarock, W. C. (2002). Time-splitting methods for elastic models using forward time schemes. *Monthly Weather Review*, 130:2088–2097.

Appendix

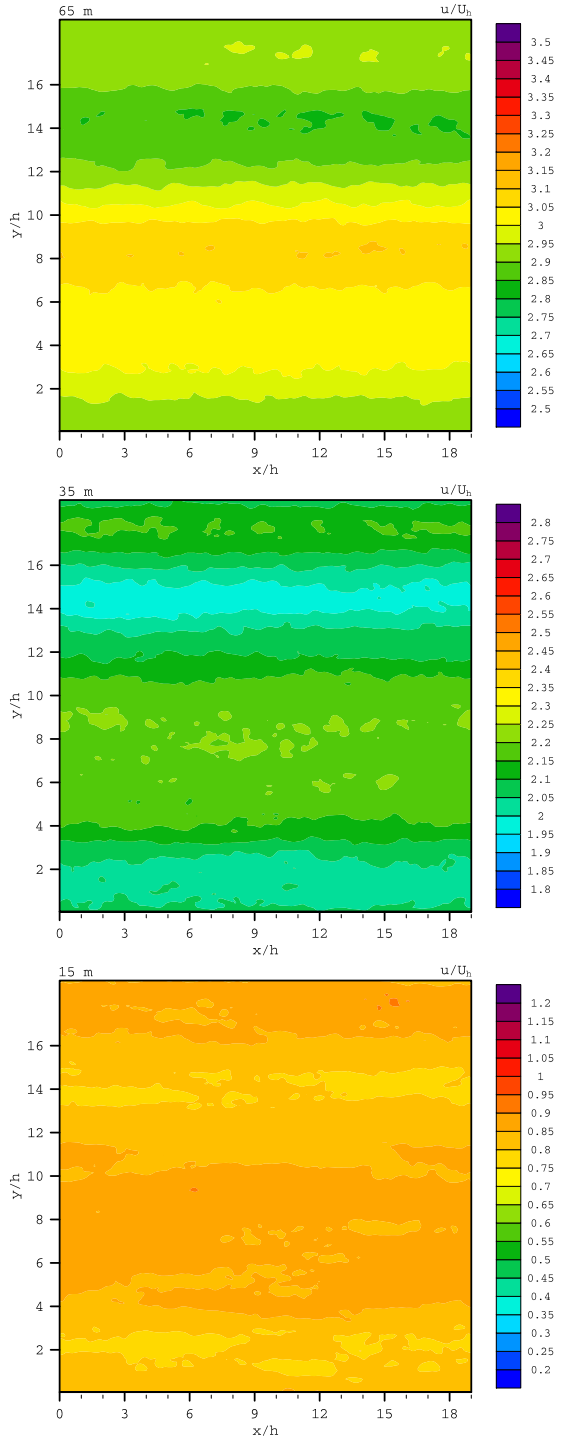

Figure 21: Cross section in the xy-plane at heights $z = 65\,\mathrm{m}$, $z = 35\,\mathrm{m}$ and $z = 15\,\mathrm{m}$, showing two hour averages of the spatial distributions of streamwise velocity. All velocities are normalized with U_h and axes are normalized with h.

Einverständniserklärung
gem. Rundschreiben A Nr. 05 / 2012 der Leibniz Universität Hannover

– Rechteverwertung für wissenschaftliche Arbeiten –

_____ _____

Name der/des Studierenden Matrikel-Nr.

ich erkläre mein Einverständnis, dass für meine ☐ Bachelorarbeit, ☐ Masterarbeit, ☐ Dissertation:

_____

die Aufnahme der Arbeit in die Hochschulbibliothek, die Fakultäts- oder Institutsbibliothek durch z.B. Überlassung der Mehrausfertigung einer Arbeit

☐ ja ☐ nein

die Vervielfältigung der Arbeit oder Herstellung von Auszügen der Arbeit für Lehrzwecke

☐ ja ☐ nein

die Veröffentlichung

☐ ja, nach Absprache ☐ nein

die öffentliche Zugänglichmachung (Veröffentlichung der Arbeit im Internet)

☐ ja ☐ nein

erfolgen kann.

_____ _____

Ort, Datum Unterschrift der/des Studierenden